APPENDIX R
EVALUATION OF AVAILABLE REFLECTION CRACKING MODELS

TABLE OF CONTENTS

LIST OF FIGURES

LIST OF FIGURES (Continued)

LIST OF TABLES

LIST OF TABLES (Continued)

INTRODUCTION

Reflection cracking is one of the primary forms of distress in hot-mix asphalt (HMA) overlays of flexible and rigid pavements. In addition to affecting ride quality, the penetration of water and foreign debris into these cracks accelerates the deterioration of the overlay and the underlying pavement, thus, reducing service life. Preliminary models for predicting the extent and severity of reflection cracking in HMA overlays have been developed. However, only limited research has been performed to evaluate and validate these models. Research is needed to address the issues associated with reflection cracking and to identify or develop mechanics-based models for use in mechanistic-empirical procedures for the analysis and design of HMA overlays. The objective of the research is to identify or develop mechanics-based models for predicting reflection cracking in HMA overlays of flexible and rigid pavements and associated computational software for use in mechanistic-empirical procedures for overlay design and analysis.

REFLECTION CRACKING–DEFINITION AND POTENTIAL MECHANISMS

Reflection cracking can be defined as the cracking of a resurfacing or overlay above underlying cracks or joints, with its probable cause being movement of some form in the underlying pavement. This cracking can result, as shown in Figure R-1, both from traffic and environmentally induced causes. The existing joints or cracks can affect reflection cracking in two potential forms (*7*):

1. The first effect of existing joints or cracks is a stress concentration at the bottom of asphalt overlay, which will lead to continued crack growth into the asphalt overlay layers.

2. If the stress-concentrating effect of the existing joints or cracks has been nullified by some means, a secondary effect of the existing joints or cracks is that maximum deflection (under wheel load) of the pavement will occur at the crack. Thus, maximum stresses in the overlay will occur at this point making it the most likely place for crack growth to initiate as an indirect effect of the existing crack.

It is well known that the first effect of existing joints or cracks−stress concentration−plays the dominant role in reflection cracking, which means that the basic mechanism causing reflection cracking is stress concentration in the overlay due to the movement in the existing pavements in the vicinity of joints or cracks. This movement may be induced by bending or shearing action resulting from traffic loads or daily and seasonal temperature changes. In fact, any reflection cracking is caused by the combination of these three mechanisms. Every pass of a traffic load will induce two shearing plus one bending effect on the HMA overlay (See Figure R-2). Moreover, these bending and shearing stresses are affected by the daily temperature. Thus, the combination of all three mechanisms is crucial to successfully model reflection cracking. In addition, crack initiation and propagation is also influenced by the existing pavement structure and conditions, reflection cracking countermeasures (e.g. reinforcing, interlayers), HMA mixture properties, the degree of load transfer at joints and cracks, and others (see Figures R-2 and R-3). Therefore, all three mechanisms and these influence factors must be taken into account in the recommended reflection cracking model.

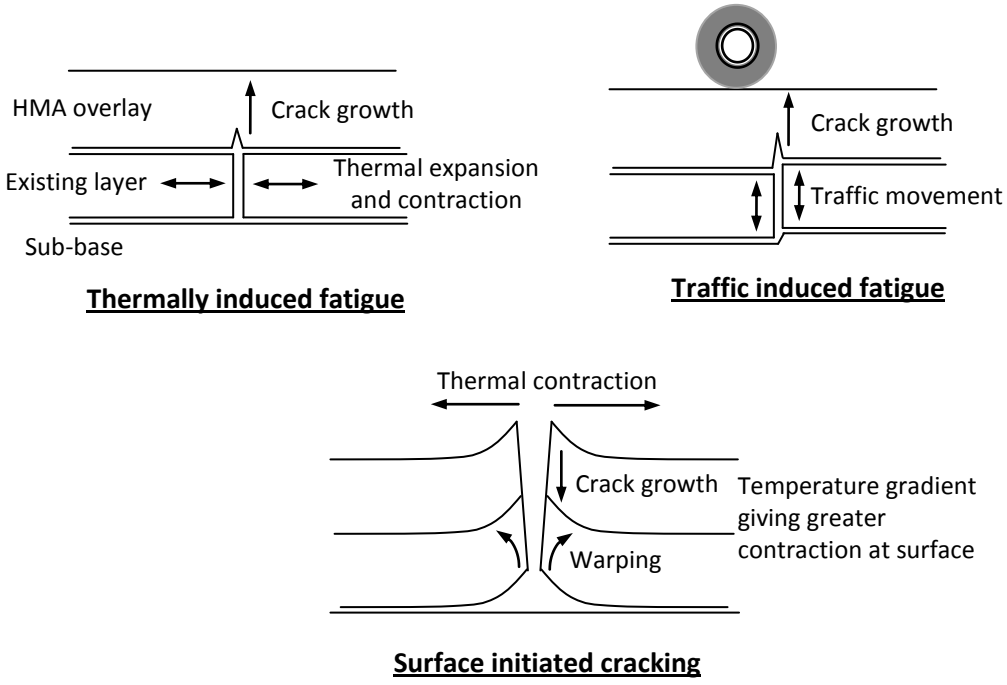

Figure R-1. Mechanisms of reflection cracking (2).

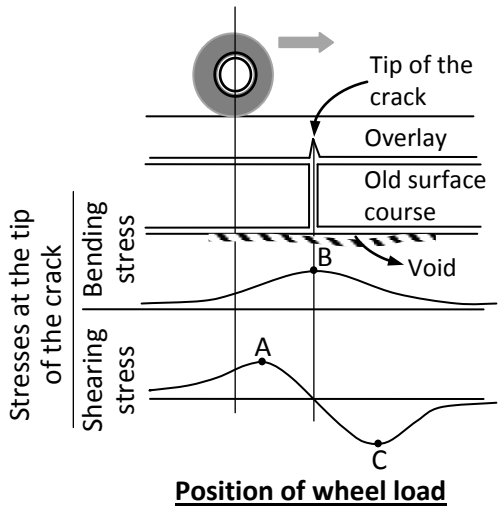

Figure R-2. Bending and shear mechanisms (3).

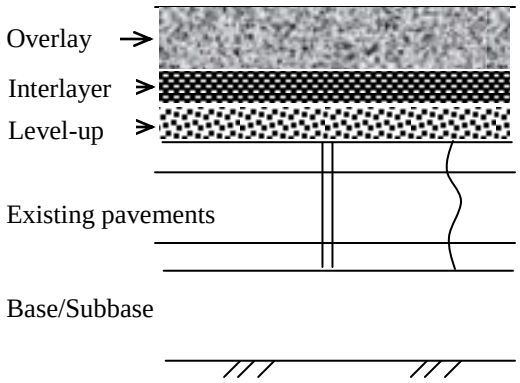

Figure R-3. Sketch of an asphalt overlay system.

AVAILABLE REFLECTION CRACKING MODELS

Reflection cracking has been a serious concern associated with asphalt overlay over existing pavements from as early as 1932, when Gary and Martin (*10*) studied this problem. Since then, many studies have been conducted to address this problem. Many models have been developed to analyze or predict reflection cracking. In general, these models can be categorized as follows:

- Empirical model
- Extended multi-layer linear elastic model
- Equilibrium equations based models
- Finite element plus traditional fatigue equation model
- Finite element plus fracture mechanics model
- crack band theory based model
- cohesive cracking/zone model
- non-local continuum damage mechanics based model

A detailed discussion of each type of model is presented in the following sections.

1. Empirical Model

A number of empirical models have been developed for predicting reflection cracking in asphalt overlay pavements. In general, these empirical models relate several variables such as existing pavement conditions, environment, and traffic loading to the amount of reflection cracking. For example, Hall, et al. (*65*) developed an empirical model to predict the total length of medium and high-severity reflection cracks in asphalt overlay pavements. The variables in the model include cumulative 80-kN equivalent single axle loads (ESALs), thickness of overlay, age of overlay, freezing index, and some measure of the condition of the PCC pavement prior to overlay.

Another empirical reflection cracking model was included in the research report of NCHRP 1-37A project (*1*). This model shown in Equation R-1 predicts the percentage of cracks that propagate through the overlay as a function of time using a sigmoidal function.

$$RC = \frac{100}{1 + e^{a+bt}} \qquad \text{(R-1)}$$

where:

RC = Percent of cracks reflected, %.

t = Time, years.

a and b = Fitting parameters shown in Table R-1.

Table R-1. Reflection cracking model parameters (8).

Pavement type	Parameters	
	a	b
Flexible	$3.5+0.75(h_{ac})$	$-0.688584-3.37302(h_{ac})^{-0.915469}$
Rigid, Good Load Transfer	$3.5+0.75(h_{ac}-1)$	$-0.688584-3.37302(h_{ac}-1)^{-0.915469}$
Rigid, Poor Load Transfer	$3.5+0.75(h_{ac}-3)$	$-0.688584-3.37302(h_{ac}-3)^{-0.915469}$

Note: h_{ac}= thickness of overlay in inches.

Obviously, this reflection cracking model (Equation R-1) is a pure regression equation. The only variables that are considered are the load transfer at joints and cracks of PCC pavements and the asphalt overlay thickness. The influences of traffic load and traffic levels, environmental condition, material properties of asphalt overlay, existing layers and subgrade, etc, are not considered at all, although these factors have a significant impact on the reflection cracking.

2. Extended Multi-layer Linear Elastic Model

Multi-layer linear elastic theory has been widely used in the asphalt pavement analysis and design. In fact, the pavement response model in the current Mechanistic-Empirical Pavement Design Guide (MEPDG) is based on multi-layer linear elastic theory. Note that the multi-layer linear elastic theory is based on the following assumptions:

- Axi-symmetrical geometry
- Homogeneous, isotropic linear elastic materials
- All layers extend to infinity in the horizontal plane

Obviously, these assumptions cannot be fully satisfied when using the multi-layer linear elastic theory to analyze an asphalt overlay over cracked pavements. Thus, the multi-layer linear elastic theory is not suitable to analyze the reflection cracking issue. However, several trials have been made to analyze the crack propagation in a simplified manner.

The approach used in the MOEBIUS software (*66*) assumes the pavement as initially sound. The asphalt overlay layer is divided in as many sublayers as possible each of which has

the initial properties of new asphalt. The first crack at the bottom is supposed to be initiated by fatigue. After the crack initiation stage, the properties of the different sublayers are progressively reduced from the bottom to the top with a rate of propagation determined from the knowledge of Paris' law. Such a procedure can obviously not claim to be able to perfectly model the complexity of the cracking phenomena. The accuracy of the predictions is, of course, limited by the oversimplification and is also dependent on the input data.

Another trial to use a multi-layer linear elastic program for crack propagation from an existing pavement through a new overlay was made by Van Gurp and Molenaar (*67*). First of all, Van Gurp and Molenaar compared analysis results from finite element analysis with those from the BISAR multi-layer linear elastic program. Based on the comparison, the finite element meshes were determined given that the critical tensile strain for an uncracked pavement structure was equal to the one calculated from the BISAR program. A study of cracked pavement structure was then conducted in order to determine an effective modulus value for the BISAR program. It was concluded that providing that reliable effective modulus values are chosen, the multi-layer linear elastic model could be used for asphalt overlay thickness design purposes.

It is clear however that this type of extension of the multi-layer linear elastic model is merely a way to use an existing tool in a field for which it was not initially developed.

3. Equilibrium Equations Based Models

An asphalt overlay design procedure has been developed for Federal Highway Administration (FHWA) and later for Arkansas State Highway and Transportation Department by McCullough and his associates (*68, 69, 70*). This procedure was based on a simple mechanistic approach in which equilibrium equations were used to estimate the stress and strain in an asphalt overlay. Moreover, this procedure has been implemented in the forms of computer programs and charts for practical overlay design. The detailed procedure is described as follows.

A. Austin Research Engineers (ARE) Procedure (68, 69)

ARE has developed an analytical procedure for reflection crack analysis based on simple static equilibrium equations without using fracture mechanics or finite element techniques. Two different failure modes are considered. The first is an opening mode (Figure R-4) due to horizontal movements of the existing concrete pavement resulting from a temperature reduction.

The second is a shearing mode (Figure R-4) resulting from a differential deflection across the joint or crack as the traffic load moves across the discontinuity. Figure R-5 presents the flow diagram of the overall reflection cracking analysis procedure. Note that the contribution to failure through the opening mode caused by bending when the traffic load is centered above the crack is not included in the procedure.

In developing the models, a number of assumptions have been made, including:

- Linear elasticity and all the assumptions associated it are applicable to this problem,
- The governing equation of static equilibrium is applicable to pavements: i. e. $\Sigma F_x=0$, $\Sigma F_y=0$, $\Sigma F_z=0$,
- Temperature variations are uniformly distributed in the existing concrete slab,
- Concrete movement is continuous with slab length,
- Movement of a layer is constant through the layer thickness, and
- Material properties are independent of space.

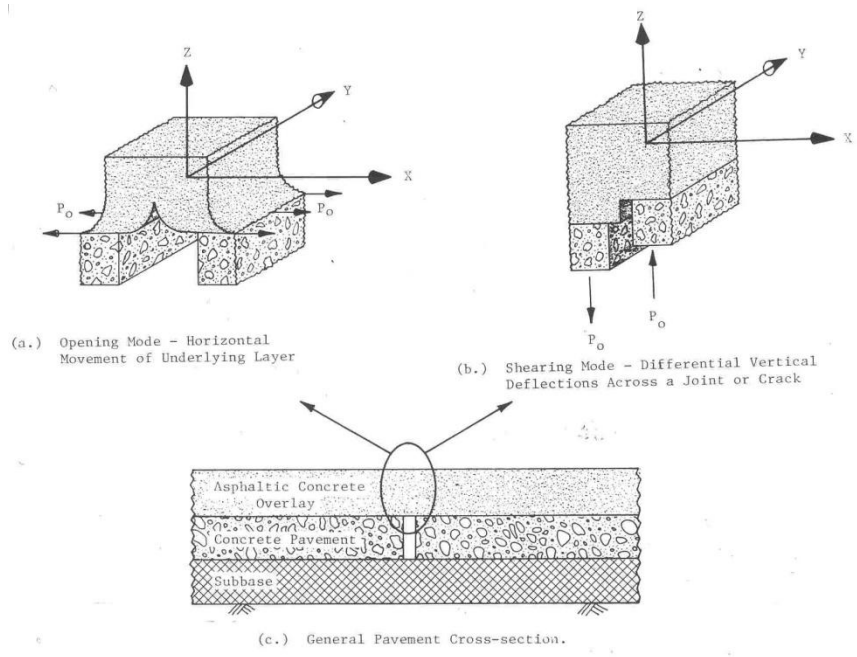

Figure R-4. Different failure modes considered for the reflection cracking model (11).

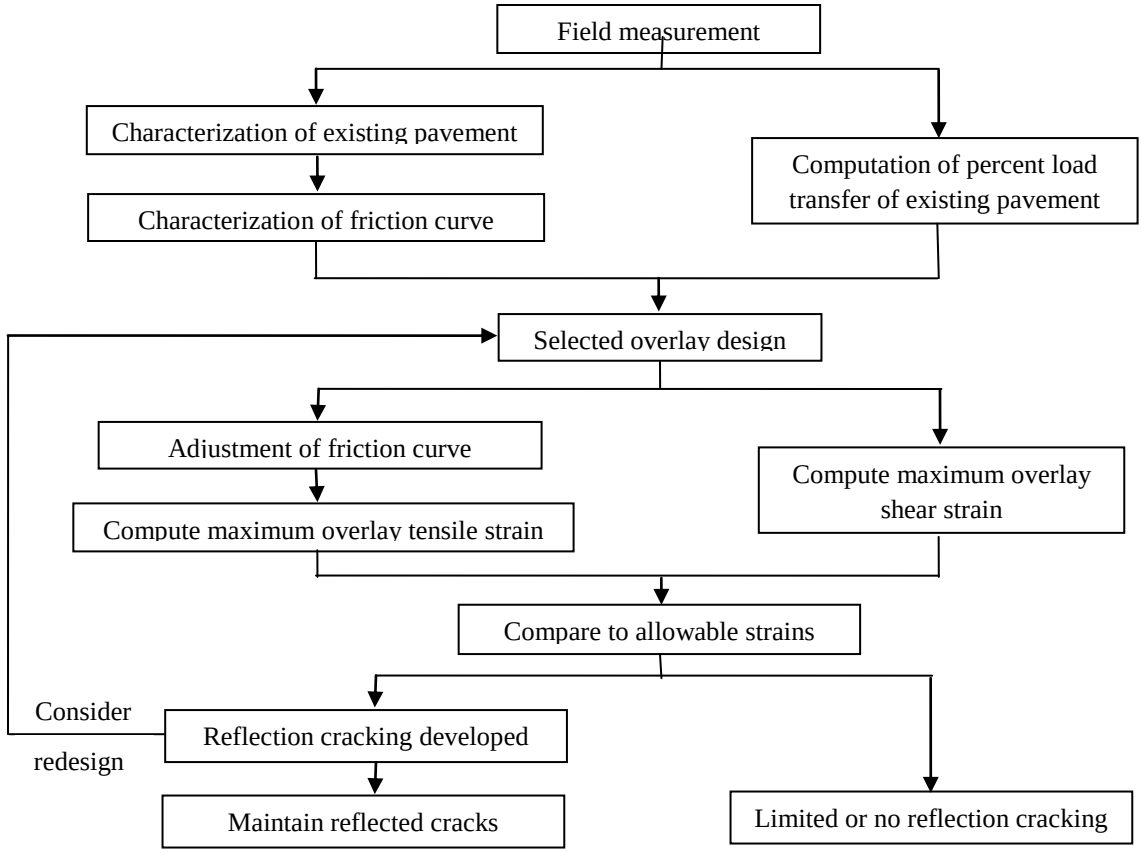

Figure R-5. Flow diagram showing the overall reflection cracking analysis procedure (68).

1) Horizontal movement and associated tensile strain

Horizontal movements are determined by characterizing the existing concrete pavement through field measurements to define a representative joint spacing and crack or joint movement associated with a specific temperature change. From this data a measure of the frictional force between pavement and underlying material is ascertained. Provision is included to modify the force-displacement relationship when an overlay is added. In addition, the effects of the use of a bond breaker at the joint or crack can be incorporated.

Movement of the existing pavement for the bonded overlay condition is expressed as:

$$Y_{cB}(x) = \alpha_c \Delta T \left[x - \beta_B x^{\beta_B} \right]_0^{X_B} \qquad \text{(R-2)}$$

and

$$Y_{cu}(x) = Y_{cB}(X_B) + \alpha_c \Delta T \left[x - \beta_u x^{\beta_u} \right]_0^{X_{BB}} \qquad \text{(R-3)}$$

where:

$Y_{cB}(x)$ = Concrete movement where the overlay and existing pavement are bonded (Figure R-6a) at a distance x from the slab's center,

$Y_{cu}(x)$ = Concrete movement where the overlay and existing pavement are unbonded (Figure R-6a) at a distance X_B+ x from the slab's center,

X_B = Distance from center of slab to the edge of the bond breaker,

X_{BB} = Width of bond breaker on one side of the joint, and

β_u, β_B = Restraint values between slabs and base for the bonded and unbonded situations.

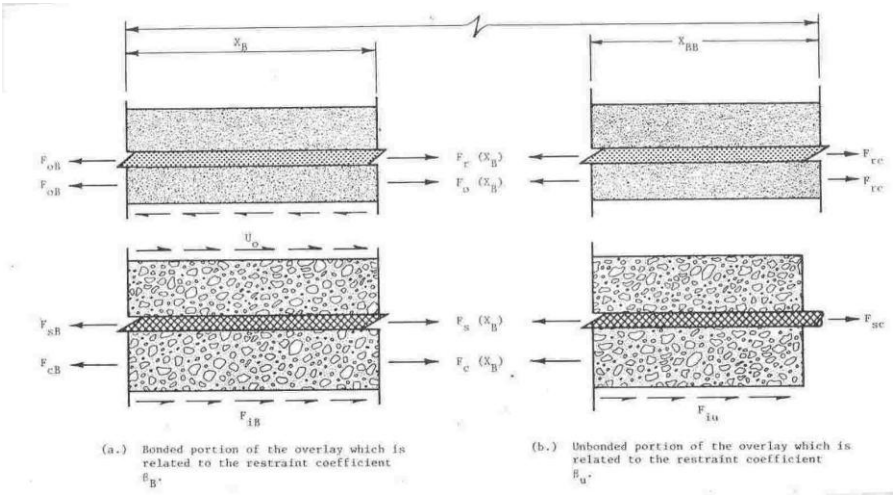

Figure R-6. Free body diagram illustrating the forces used in evaluating a bonded overlay for reflection cracking potential (68).

For the various materials and different asphaltic concrete mix designs, the force transferred from the existing pavement to the asphalt overlay is related to concrete movement in the form of a force-displacement curve, between the concrete slab and subbase, or is in the form

of bonding forces caused by slippage between the concrete and the steel. No data are available to adequately define a relationship to explain the force transfer between the two materials. Therefore, two purely theoretical conditions were used to estimate this relationship. *The first* assumes, in the section where concrete slab and asphalt overlay are bonded, concrete pavement movement equals movement of the asphalt overlay, and is constant with pavement thickness. Asphalt concrete is a viscoelastic material that approaches an elastic state at low temperatures. The critical conditions occur at these low temperatures; hence, the above assumption was believed to be reasonable. *The second* uses an average bonding stress between the asphalt overlay and the existing surface, in the section where the existing concrete pavement and asphalt overlay are bonded, to compute the force transferred between the two layers.

$$U_0 = 12\mu_0 X_0 \qquad \text{(R-4)}$$

where:

- U_0 = Force transferred between overlay and existing pavement layers; load per unit width, e.g., kN/m,
- μ_0 = Average bonding stress between the overlay and existing pavement; theoretical values for asphalt concrete overlays are provided, and
- X_0 = Distance over which slippage occurs between overlay and existing surface in the bonded overlay.

Various values of the restraint coefficient are selected until the frictional, concrete, and asphalt overlay forces balance (Figure R-5), determining the horizontal tensile strain in the overlay above the joint or crack.

$$\varepsilon_{oc} = \frac{F_{oc}}{A_o E_o} \qquad \text{(R-5)}$$

where:

F_{oc} = Force in the overlay at a joint or crack,

A_o = Cross-sectional area of the overlay, and

E_o = Stiffness of the asphalt concrete overlay at a comparatively long time of loading.

Finally, this horizontal tensile strain can be computed for various temperatures and compared to an allowable tensile strain to determine if temperature related reflection cracks will occur. Using this technique, reflection cracking due to environmental effects and concrete movement can be predicted to provide an analytical approach to predict the performance of an overlay system.

2) Differential vertical movement and associated shear strain

To consider the effects of differential vertical movements, deflections are measured on each side of the joint or crack for a load applied to one side and the load transfer, L_T, is estimated from the expression:

$$L_T = 1 - \frac{W_l - W_u}{W_l} \qquad \text{(R-6)}$$

where:

W_l = Deflection measured at the joint on the loaded slab, and

W_u = Deflection measured at the joint on the unloaded slab.

The shear force in the overlay at the joint is then determined:

$$P_o = L_D(1 - L_T) \qquad \text{(R-7)}$$

where:

P_o = Shear load, and

L_D = Design load.

Shear stress in the asphalt overlay, τ_0, is estimated by assuming a constant shear force over the width of the applied load:

$$\tau_o = \frac{P_o}{D'_o W} \qquad \text{(R-8)}$$

where:

D'_o = Effective asphalt overlay thickness, and

W = Width of the applied load.

The corresponding shear strain, γ_o, is calculated from the following expression:

$$\gamma_o = \frac{2\tau_o(1+\upsilon_o)}{E_o} \qquad \text{(R-9)}$$

with E_o and υ_o being the elastic constants (measured at a short time of loading) for the asphalt concrete overlay.

The value so estimated is then compared to a limiting value for shear strain which presumably is developed from experience.

B. <u>Extended ARE Procedure (*69*)</u>

The ARE procedure above was then extended and calibrated for the Arkansas State Highway and Transportation Department (*70*). It was recognized that the tensile strains that induce reflection cracking come about as the result of both direct thermal stresses and the temperature-drop-related movements of the underlying slab, and the temperature variations are cyclic in nature, the reflection cracking in asphalt overlays must be attributed to fatigue or the accumulation of damage brought about by cyclic loading. Therefore, it was decided that the

fatigue damage concept was incorporated into the computer program: ARKRC-2. A fatigue equation for temperature-related movements (Equation R-10) was developed on the basis of a calibration of observed overlay performance in Arkansas and Texas.

$$N_T = a_1(\varepsilon_T)^{a_2} \quad \text{(R-10)}$$

where:

N_T = Average number of fixed strain cycles needed to develop a reflection crack at a given location,

ε_T = Asphalt concrete overlay tensile strain from a given critical temperature drop,

a_2 = -3.70,

a_1 = 8.072 x 10-4 (EOV)-1.118, and

EOV = Asphalt concrete overlay creep modulus (psi).

To consider the variable load effects (such as that resulting from varying low temperature drops), the following Miner's linear damage law was used:

$$D = \sum_{i=1} \frac{n_i}{(N_T)_i} \quad \text{(R-11)}$$

where:

n_i = Average number of days during the year on which the overlay is subjected to a given strain level $(\varepsilon_T)_i$, and

$(N_T)_I$ = Allowable number of cycles of a given strain the overlay can carry before it cracks.

For differential vertical movement and associated shear strain, several expansions were also made. For example, the maximum shear stress at the neutral axis of the cross section was estimated in the form of following equation.

$$\tau_{max} = \frac{3V}{2bh} \quad \text{(R-12)}$$

where:

V = V_o, i. e. overlay shear force (lb),

b = Width of the section (in.); for purposes of the overlay shear calculations, this value should be the width of the region of shear, which is approximately 25 inches for a dual-tired axle, and

h = height of cross section (in.), for the effective overlay thickness for overlay shear calculations.

The maximum shear strain in the asphalt overlay (γ_{OV}) is determined by using the following equation:

$$\gamma_{OV} = \frac{\tau_{OV}}{G_{OV}} \quad \text{(R-13)}$$

where $\tau_{OV} = \tau_{max}$, the maximum shear stress in the asphalt overlay (psi), and G_{OV} is the overlay shear modulus (psi).

Finally, the overlay life for a given shear strain is determined by using a fatigue-type relationship based on asphalt shear strain. Based on the work done by Anagnos and Kennedy (*71*), an alternative shear fatigue equation (Equation R-14) was developed, because there was no such a shear fatigue model in the literature.

$$\gamma_{OV} = 0.7587 \bullet (EDV)^{-0.3002} \bullet (N_T)^{-0.2703} \quad \text{(R-14)}$$

where N_T = DTN18, the design 18-kip ESAL applications that will be carried by the overlay before the development of reflection cracking; and EDV is the dynamic modulus of the overlay material (psi).

4. Finite Element Plus Traditional Fatigue Equation Model Approach

Finite element (FE) techniques have been widely used to analyze reflection cracking of asphalt overlays. This section will focus on finite element methodology without the application of fracture mechanics. The FE plus fracture mechanics approach will be discussed in the next section.

A. Monismith and His Associates' Work

Monismith and Coetzee (*7*) made a comprehensive review on reflection cracking, including analysis, laboratory studies, and design considerations in 1980. One of their conclusions is that "although fracture mechanics applications are conceptually appealing and undoubtedly have the potential to provide solutions for crack reflection through pavement overlays, these solutions are not yet available in a form which is immediately useful or adequate for design purpose." (It should be noted that this conclusion was drawn in 1980 rather than today.) Thus, the recommendation was to use the standard FE to examine the state of stress/strain rather than the stress intensity factor (SIF) at a crack in the existing pavement. These stress/strain levels can then be used with standard fatigue analysis for prediction of asphalt overlay life. For example, Figure R-7 presents a reflection cracking design subsystem proposed by Monismith and Coetzee (*7*).

Coetzee and Monismith (*72*) have utilized the 2-D finite element procedure to examine the distribution of stresses in an overlay in the vicinity of a crack with and without an asphalt rubber membrane (SAMI). For a specific load applied to the surface of the overlay directly above the crack, the influence of a number of variables on the resulting stresses has been ascertained, including: thickness and stiffness of the asphalt rubber layer; asphalt concrete overlay thickness and stiffness; stiffness of the existing cracked layer; crack width in the existing surface. In addition, stresses in the vicinity of the crack have been ascertained for a temperature reduction of 40 F (22.2℃) at the surface of the overlay.

To analyze the pavement structure for traffic loads, the finite element program termed ANSR-I was utilized; the finite element idealization of the pavement structure, Figure R-8a, is shown in Figure R-8b. The effect of overlay thickness and asphalt rubber membrane on effective stress is shown in Figure R-9.

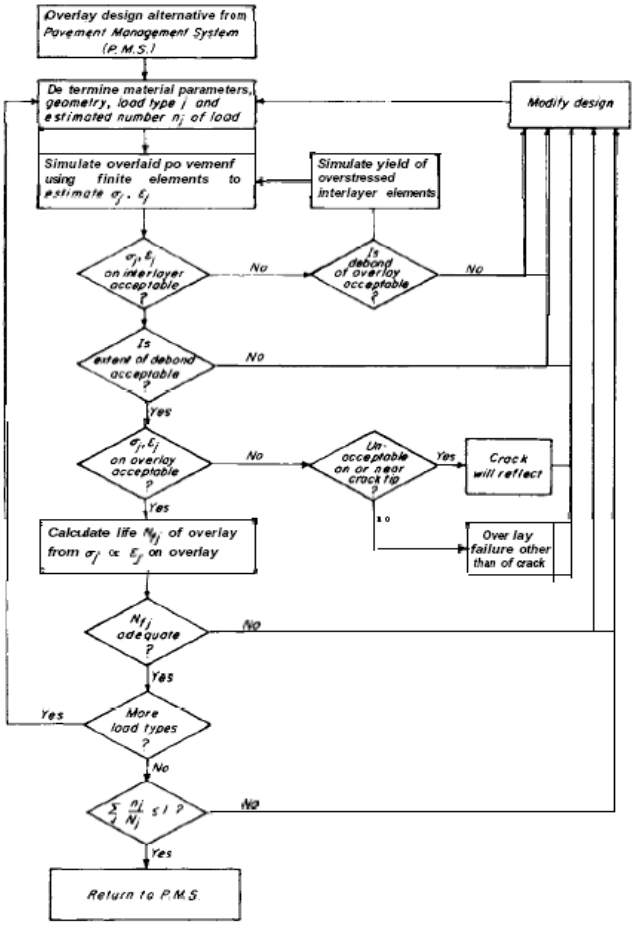

Figure R-7. Reflection cracking design subsystem (7).

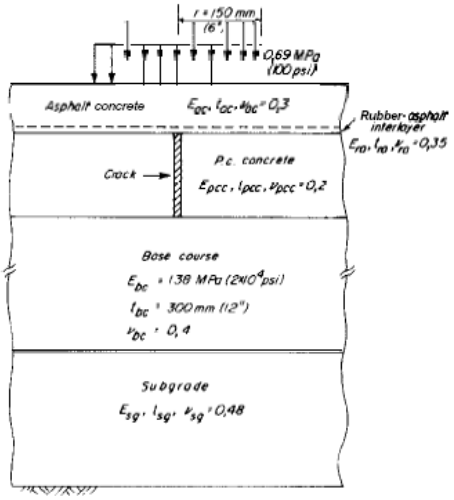

Figure R-8a. Schematic representation of pavement structure (7).

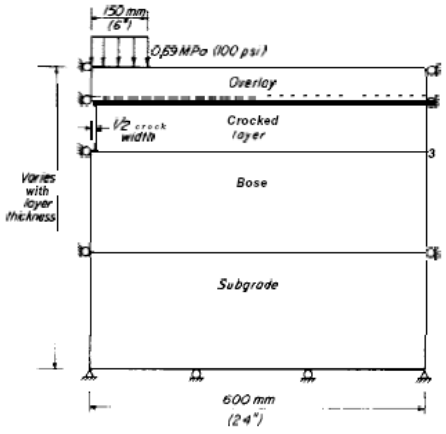

Figure R-8b. Schematic finite element representation (7).

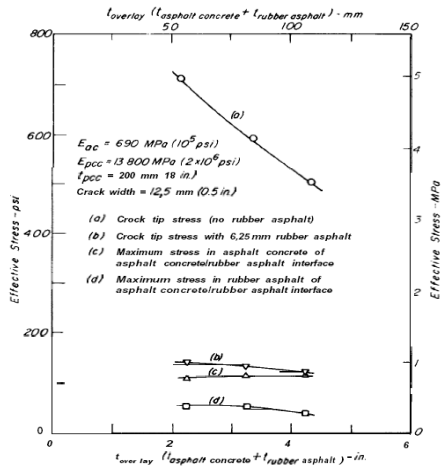

Figure R-9. Effect of overlay thickness on effective stress at crack tip (7).

The most recent work on reflection cracking done by Monismith and his associates was California's Interstate-710 rehabilitation project (*73*). In this rehabilitation project, FE analyses were performed to calculate strains under traffic loads at the bottom of thicker overlays, then to relate those to strains leading to long fatigue life in beam fatigue tests.

B. *Chen et al.'s work*

In early 1980s, Chen et al. (*74*) also used 2-D linear plane strain FE program to analyze the Arizona's three-layer overlay system of rigid pavements under moving traffic loads (shown in Figure R-10). The analysis results indicated that shearing action is more inductive to reflection cracking of overlays than bending action when a traffic loading is moving from one side of a joint to the other.

C. *Francken and his associate's work*

In the early 1990s, Francken and Vanelstraete (*75*) used 2-D FE methodology to analyze the effect of interface systems on preventing reflection cracking. Later, Vanelstraete and Francken (*76*) compared the 2-D FE results with those of 3-D FE. Figure R-11 shows the significant difference between 2-D and 3-D. 2-D plane strain FE provides a much higher strain, which is understandable because the load is assumed to act on the whole pavement cross-section. This difference highlights the importance of using 3-D FE analysis.

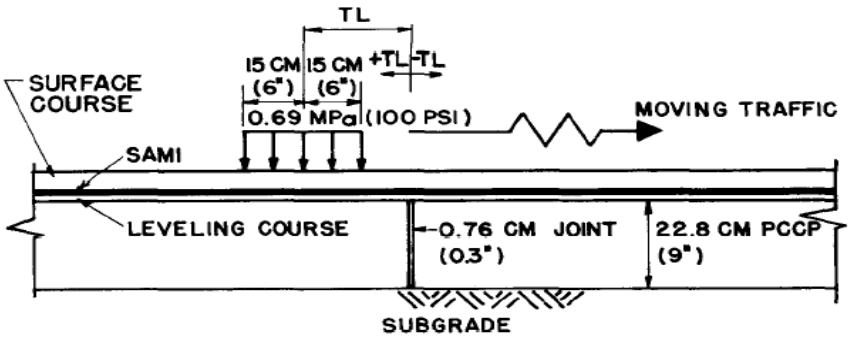

LOADING CASE		A	B	C	D	E	F	G	H	I	H'	G'	F'	E'	D'	C'	B'	A'
TL	(CM)	40	35	30	25	20	15	10	5	0	-5	-10	-15	-20	-25	-30	-35	-40
	(IN)	16	14	12	10	8	6	4	2	0	-2	-4	-6	-8	-10	-12	-14	-16

Figure R-10. General configuration of the overlay system on rigid pavement (15).

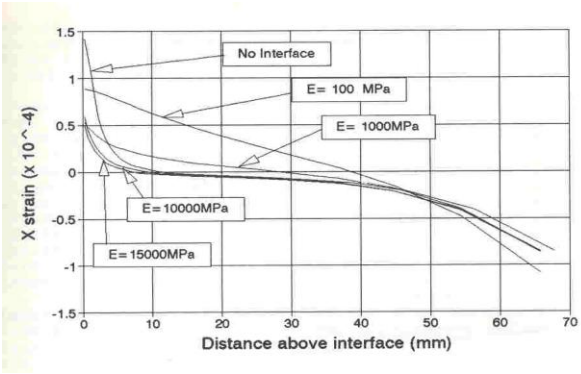

Figure R-11a. 2-D FE Simulation.

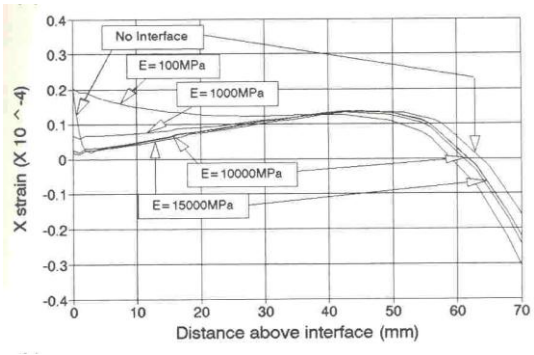

Figure R-11b. 3-D FE Simulation.

Figure R-11. Calculated x-strain as a function of distance above interface for different stiffness of the interface (76).

D. *Buttlar and his associates' work*

In 2002, Kim and Buttlar (*77*) also conducted a detailed analysis of the critical response in an asphalt overlay system for Taxiway E at the Greater Peoria Regional Airport (GPRA) using a 3-D nonlinear FE program. Figure R-12 illustrates typical trends in the development of longitudinal stresses and shear stresses in an untreated asphalt overlay system subjected to DC-8 aircraft traffic load and environmental loads. The results presented were based upon a rigorous 3-D nonlinear FE analysis. Consider the longitudinal stress pattern for an untreated overlay system subjected to DC-8 loading. As expected, a very high longitudinal tensile stress occurs at the bottom of the overlay, directly above the existing crack site. The tensile stress in the overlay under these conditions [17,065 kPa (2,475 psi)] would exceed the tensile strength of a typical hot-mix asphalt by a factor of 5–6. This result clearly demonstrates the necessity of reflection crack treatment. Otherwise, rapid reflective crack propagation would be expected.

Bozkurt (*78*) quantitatively illustrated how interlayers such as ISAC reduce critical overlay responses that are related to reflection crack development. Field deflection testing, pavement instrumentation, fundamental laboratory testing, and three-dimensional nonlinear finite element modeling was performed in conjunction with the Rantoul National Aviation Center Demonstration project to better understand the key mechanisms of reflective cracking and to evaluate promising mitigation techniques. Modeling results indicate that ISAC nearly eliminates stress development in the bottom of the asphalt overlay due to joint opening and closing due to temperature cycling, and is particularly beneficial for thinner overlays.

E. *Sousa et al.'s work*

In 2005, Sousa et al. (*79*, *80*) presented a mechanistic-empirical based overlay design method for reflective cracking, which is a condensed version of an eight chapter, 200-page report, entitled "Development of a Mechanistic Overlay Design Method Based on Reflective Cracking Concepts (*81*)." A methodology was proposed for the design of overlays on existing, cracked flexible pavements to minimize the risk of premature reflective cracking. The proposed overlay design method consists of the seven steps presented below. Currently, the model has been calibrated for only two asphalt overlay materials: dense graded mixes with PG70-10 binders (HMA-DG) or gap graded mixes with asphalt rubber modified binders (AR-HMA-GG). The

asphalt rubber binder must be produced using the "wet" process and it must contain approximate 19-20 percent crumb rubber.

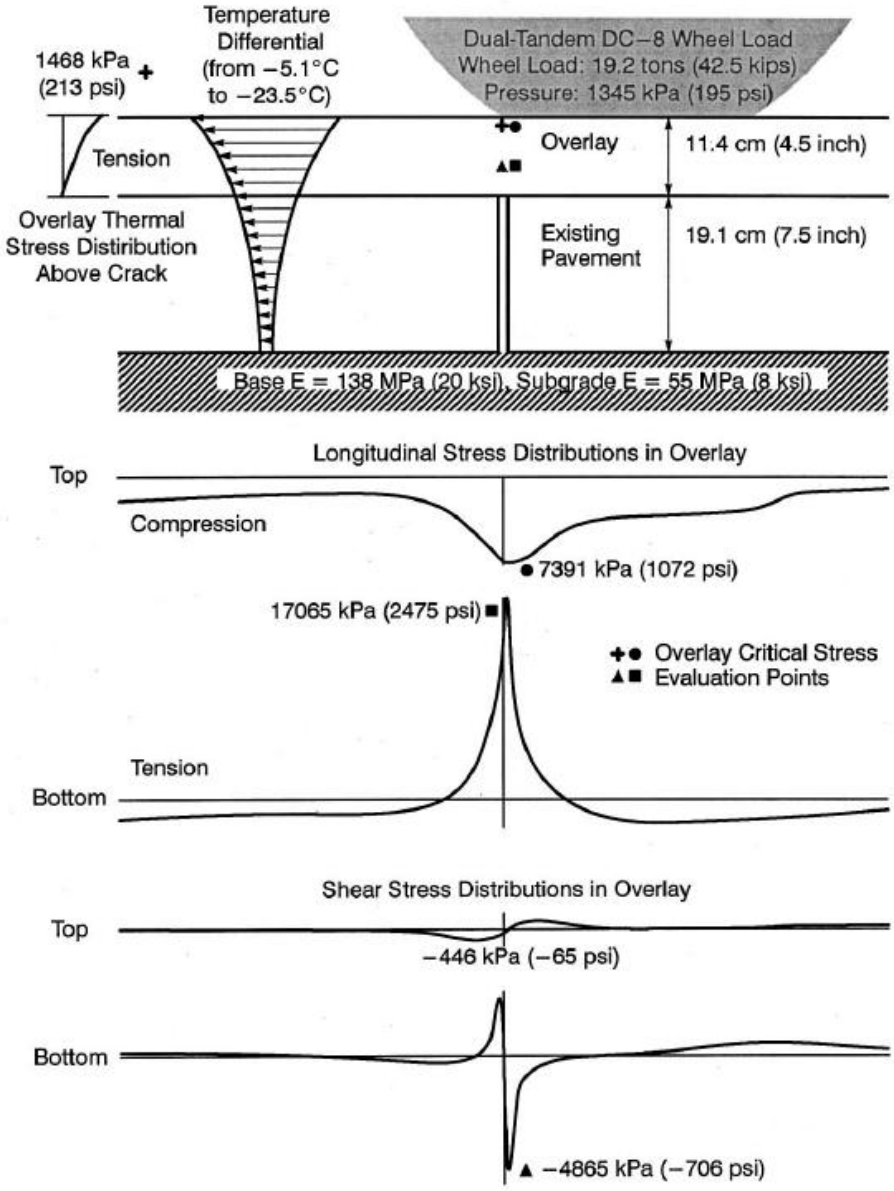

Figure R-12. Stress distribution of untreated overlay system (70).

1) Determination of the Moduli and Thicknesses of the Pavement Section Layers

This can be accomplished using FWD backcalculation methods or other forms of estimating cracked pavement section moduli. Care must be taken in the selection of modulus representative of the most damaged sections. As such, the 90th or 95th percentile of deflections (or backcalculated moduli) should be selected. Coring for determination of layer thicknesses should be carried out as close to the locations where the 90-95th percentile FWD test points were selected.

2) Determination of Representative Air Temperatures

The maximum and minimum air temperature determined with the desired reliability should be obtained for the location where the pavement is to be overlaid. Furthermore, it is necessary to compute the mean average monthly air temperature as proposed by the Shell design method (*81*).

3) Selection of Design Cracking Percentage

The percent cracking should be keeping with that previously discussed. The value selected should be in keeping with an agencies overlay policy. Arizona Department of Transportation generally has observed less than five percent cracking over a period of ten years when an asphalt rubber surface mix is used.

4) Determination of Adjustment Factors

During the process of model calibration, several adjustment factors were developed: an aging adjustment factor (AAF), a temperature adjustment factor (TAF) and a field adjustment factor (FAF). These three adjustment factors need to be considered for the location where the overlay will be placed and for the desired cracking level at the end of the overlay's design life.

These adjustment factors are discussed as follows:

The AAF was introduced to capture the effect of aging in the overlay as a function of the maximum air temperature. The AAF can be determined from the following Equation R-15 for HMA-DG mix or Equation 16 for AR-HMA-GG mix. These AAFs are applicable for maximum air temperatures ($T_{max\text{-}air}$) between 35℃ and 50℃.

$$AAF = 0.0363*T_{max\text{-}air} + 0.3000 \quad \text{(R-15)}$$

$$AAF = 0.0088* T_{max\text{-}air} + 0.8800 \quad \text{(R-16)}$$

The TAF was used to consider the low temperature effect on reflection cracking, because this effect was not taken into account separately in the proposed design method. The TAF can be determined from Equation R-17 for HMA-DG mixes or Equation 18 AR-HMA-GG mixes (wet process only). This method is applicable for Reflective Cracking Temperatures (RCT) between-10℃ and +10℃. The RCT was arbitrarily set as the mean value between the minimum air temperature ($T_{min-air}$) and the average mean air monthly temperature ($T_{av-mean-air}$)

$$TAF = -0.0900*RCT + 2.5500 \quad \text{(R-17)}$$

$$TAF = -0.0720 * RCT + 1.7448 \quad \text{(R-18)}$$

where:

$$RCT = T_{max-air} + 0.5 * (T_{av-mean-air} - T_{min-air})$$

The FAF was introduced to relate the predictions obtained using the empirical-mechanistic reflection cracking model with actual (reported and observed) field performance. The FAF can be computed from the following equation:

$$FAF = e^{0.2303* PC} \quad \text{(R-19)}$$

where:

PC = Cracking Percentage between 2 percent and 10 percent.

Actually, the determination of the three factors: AAF, TAF and FAF was done simultaneously, iteratively and interactively, and combining these three factors in a logical fashion involved engineering judgment considerations.

5) Selection of Overlay Material Modulus

Two types of materials for the overlay may be selected: Conventional HMA-DG or AR-HMA-GG. For these two materials, the modulus and flexural fatigue life are obtained through flexural fatigue tests as shown in Figure R-13. Other moduli can be computed and

introduced in the method based on actual tests performed on other types of materials. However, it must be assumed that the TAF or the AAF will either be identical to that of the HMA-DG material or the ARHMA-GG material.

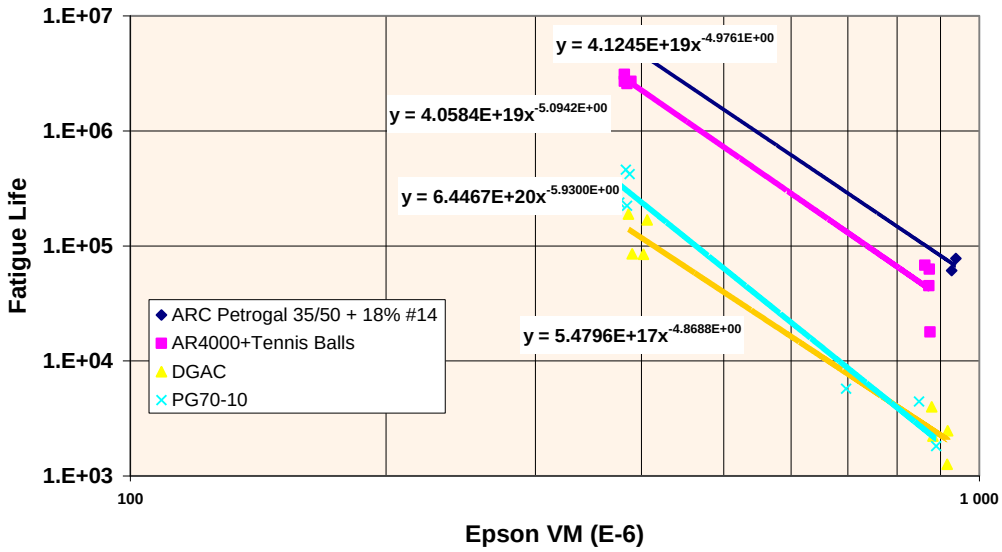

Figure R-13. Flexural fatigue life as a function of Von Mises Strain-ε_{VM} (81).

6) Determination of the Design Value, ε_{VM}

A 3-D FE program was used to analyze the state of stress/strain in the zone above a crack. Figure R-14 presents the 3-D mesh used for the analyses. In this figure, a longitudinal crack is represented for a pavement with four layers, i.e., an overlay layer placed on a bituminous cracked layer, a granular layer, and the subgrade layer. The influence of pavement characteristics on the state of stress/strain was made defining a deviator strain, called the "Von Mises" strain. Von Mises strain-ε_{VM} was calculated as expressed in Equation R-20.

$$\varepsilon_{VM} = \sqrt{\frac{1}{2}\left[(\varepsilon_1 - \varepsilon_2)^2 + (\varepsilon_1 - \varepsilon_3)^2 + (\varepsilon_2 - \varepsilon_3)^2\right]} \qquad \text{(R-20)}$$

where:

ε_{VM} = "Von Mises" strain, and

ε_1, ε_2, ε_3, = Principal strains,

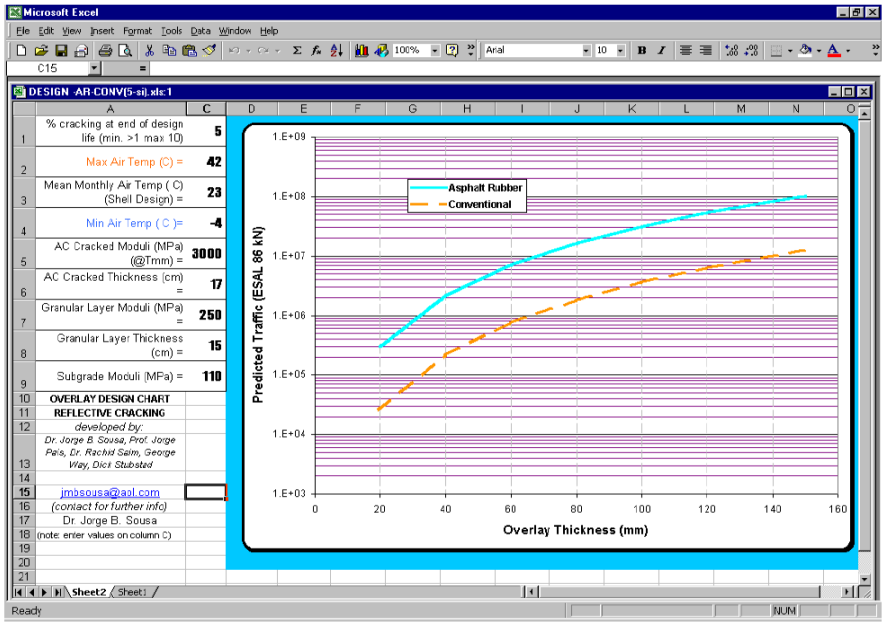

Figure R-14. Overlay design against reflection cracking (80).

Based on analysis results on 384 pavement structures, a statistical model for ε_{VM} was developed the following forms.

$$\varepsilon_{VM}\,(1\text{x}10^{6}) = a * [\textit{Overlay thickness}]^{b} \qquad \text{(R-21)}$$

$$a = \prod_{i=1}^{6}\left[a_{1i} * \ln(X_i) + a_{2i}\right] \qquad \text{(R-22)}$$

$$b = \prod_{i=1}^{6}\left[b_{1i} * \ln(X_i) + b_{2i}\right] \qquad \text{(R-23)}$$

where:

a_{ij}, b_{ij} = Coefficients given in Table R-2, and

X_i = Pavement properties namely thickness and moduli. These values must be introduced by the order defined in Table R-3.

Table R-2. Statistical coefficients a_{ij}, b_{ij} for the ε_{VM} model (80).

i	a_{1i}	a_{2i}	b_{1i}	b_{2i}
1	-1.038E-04	-1.446E-01	7.169E-03	1.314E-01
2	2.777E-01	-4.022E+00	9.773E-05	-6.368E-01
3	-1.173E+00	1.212E+01	-4.946E-01	7.069E+00
4	1.281E+00	5.070E-01	3.923E-02	2.641E+00
5	-5.160E-01	6.964E+00	3.265E-02	-1.287E+00
6	-1.775E-01	2.385E+00	1.875E-03	-8.167E-01

Table R-3. Variables defining the pavement properties in Equations 22 and 23 (80).

i	X_i	Minimum	Maximum
1	Thickness of the existing cracked layer (m)	0.10	0.25
2	Thickness of the granular layer (m)	0.20	0.40
3	Modulus of the overlay layer (MPa)	2000	10000
4	Modulus of the existing cracked layer (MPa)	2000	3500
5	Modulus of the granular layer (MPa)	150	450
6	Modulus of the subgrade layer (MPa)	50	150

Note that the modulus of the overlay layer must be multiplied by the computed AAF. With the modulus and thickness for each layer, the ε_{VM} value for the overlay is determined using Equations R-21, R-22, and R-23. Also, the ε_{VM} value obtained through these equations must be multiplied by 86/132 (to convert ε_{VM} from 130-kN to 80-kN axle loads), and also by the TAF. The value obtained in this process is thus the design ε_{VM}.

7) Determination of Design Equivalent Standard Axle Loads

Using the appropriate flexural fatigue equation as introduced in Figure R-13, determine the number of equivalent standard axle loads (ESALs) that can be sustained by the overlay prior to the onset of reflective cracking, i.e.:

$$ESALs = 4.1245E19 * [\varepsilon_{VM} (1x10^{-6})]^{-4.9761} \qquad \text{(R-24)}$$

for asphalt rubber binders derived through the wet process, with a 19% -20% binder content and a gap-graded mix, or:

$$ESALs = 6.4467E19 * [\varepsilon_{VM} (1x10^{-6})]^{-5.9300} \qquad \text{(R-25)}$$

for conventional PG70-10 binders and dense graded mixes.

Multiply the design ESALs by the FAF computed in Step 4. The resulting number should represent the number of ESALs required for the overlay to reach the selected percentage of cracking. Other fatigue curves can be determined and used by this method, based on actual flexural fatigue tests performed on the specific asphalt (whether conventional or modified) material type proposed with due consideration to all adjustment factors.

Finally, this overlay design method, as shown in Figure R-14, was coded into an EXCEL spread sheet which contains all the formulas presented above. The input values are entered in column C and the graph regenerates itself for the new pavement and environment conditions selected. From the demanded traffic the required thickness can be determined for conventional and asphalt rubber mixes. Generally in most cases the asphalt rubber mix will give an overlay about half as thick as the conventional mix for the same design traffic level.

The essential part of the proposed overlay design method is to calculate the stress/strain field, then relate the stress/strain above the crack to the beam fatigue equation, which is similar to Monismith and his associates's approach (*7*, *73*). However, there are several differences. One of the differences is that Sousa et al. used the Von Mises strain instead of tensile strain above the crack. In addition, because Sousa et al. realized that using an FE program in a routine design is too time consuming and requires knowledge beyond the training received by average pavement engineers, a statistical model was developed to evaluate the critical Von-Mises strain. In summary, this practical design method can be used in routine design. However, several limitations also exist in the method.

One limitation of such an approach is that no effort was made to explicitly account for crack propagation. Fatigue life of a beam in the beam bending test is defined as the time required for a beam to reach 50 percent reduction for the overall stiffness, which roughly corresponds to the time when the first major crack is initiated in the beam. As stated by Wu (*82*), "The concept of crack initiation is somewhat ambiguous in the case of reflective cracking since there are pre-existing cracks in the underlying cracked/jointed layer. If the overlay is perfectly bonded with the underlying layer, there should be no crack initiation stage at all." Wu (*82*) made an effort to establish a correlation between the fatigue life calculated by the fatigue equation, denoted as N_{FAT}, and the crack through time of the overlay calculated by FE simulation with an advanced non-local continuum damage mechanics model for the Asphalt concrete mixes, denoted as N_{CDM}. (Note that N_{FAT} is no longer interpreted as the crack initiation time, rather it is simply an indicator of the susceptibility of a particular overlay to reflection cracking.) Figure R-15 illustrates the relationship between N_{CDM} and N_{FAT}. Surprisingly, only a very weak correlation exists between N_{CDM} and N_{FAT}. The correlation coefficient turns out to be only 0.45 between $\log N_{CDM}$ and $\log N_{FAT}$. Wu's results (*82*) clearly indicate the limitation of the beam fatigue equation based reflection cracking model, and the necessity of considering cracking propagation. Crack propagation is discussed in the following sections.

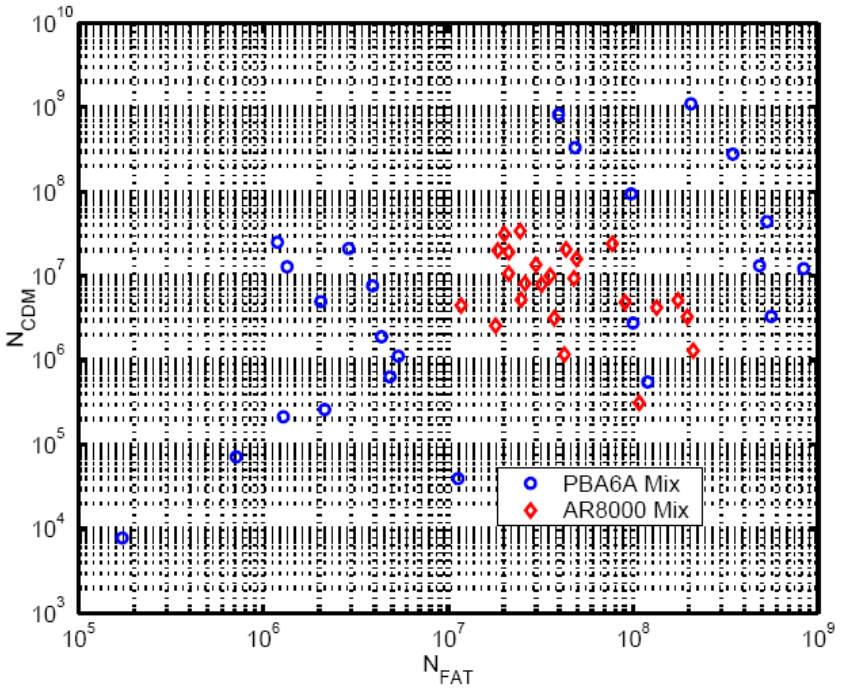

Figure R-15. Comparison between N_{CDM} and N_{FAT} (80).

5. *Finite Element Plus Fracture Mechanics Model*

Since Majidzadeh (*48*) introduced fracture mechanics concepts into the field of pavements, the fracture mechanics approach has been widely used in predicting pavement cracking, especially reflection cracking analysis. As stated by Monismith et al. (*7*), "Fracture mechanics applications are conceptually appealing and undoubtedly have the potential to provide solutions for crack reflection through pavement overlays." In fact, Lytton and his associates (*12, 52, 83, 84, 85, 86, 87*) have successfully applied facture mechanics to predict reflection cracking of asphalt overlays since mid-1970s. The same fracture mechanics concept was also used by Owusu-Antwi et al. (*49*) and Al-Qadi and his associates (*50, 88*).

Different from continuum mechanics, the fracture mechanics approach focuses on crack propagation. The occurrence of reflection cracking is a crack propagation process caused by a combination of the three modes of loading (Figure R-16):

- Mode I loading (opening mode, K_I) results from loads that are applied normally to the crack plane (thermal and traffic loading).

- Mode II loading (sliding mode, K_{II}) results from in-plane shear loading, which leads to crack faces sliding against each other normal to the leading edge of the crack (traffic loading).
- Mode III loading (tearing mode, K_{III}) results from out-of plane shear loading, which causes sliding of the crack faces parallel to the crack leading edge. Compared to Modes I and II, Mode III is rare and is often neglected for simplicity.

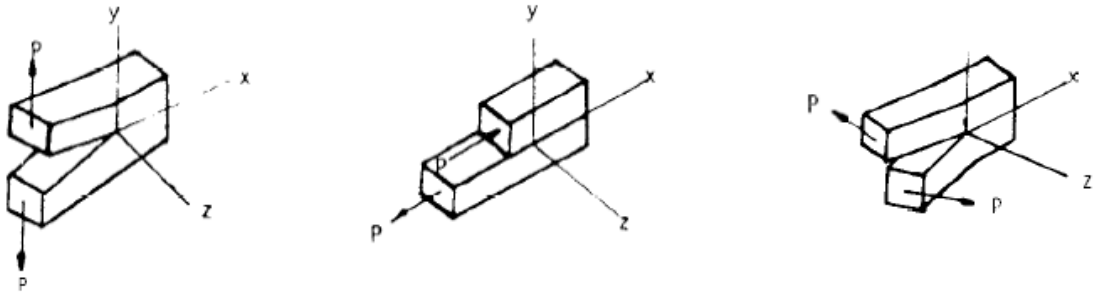

(a) (b) (c)

Figure R-16. Three modes of crack opening displacement: (a) Mode I−Opening Mode, (b) Mode II−Shearing Mode, (c) Mode III−Tearing Mode (52).

The fact that the mechanisms of reflection cracking (bending, shearing and thermal stresses) discussed previously, can be exactly modeled by fracture Modes I and II makes the fracture mechanics approach the best option for modeling reflection cracking.

The generally accepted crack propagation law was proposed by Paris and Erdogan (*11*) in the form of Equation R-26. It has successfully been applied to asphalt concrete by many researchers, for the analysis of experimental tests and prediction of reflection cracking and low temperature cracking.

$$\frac{dc}{dN} = A*(\Delta K)^n \qquad \text{(R-26)}$$

where:

c = Crack length,

N = Number of loading cycles,

A, n = Fracture properties of asphalt mixture determined by the experimental test, and

ΔK = Stress intensity factor (SIF) amplitude, depending on the geometry of the pavement structure, fracture mode, and crack length.

The number of load cycles N_f needed to propagate a crack through an asphalt overlay of thickness *h* can be estimated by numerical integration in the form of Equation R-27.

$$N_f = \int_0^h \frac{dc}{A(\Delta K)^n} \qquad \text{(R-27)}$$

It is apparent that the SIF, material fracture properties (A and n), and interlayer properties (if used) must be known in order to predict the reflection cracking performance of an asphalt overlay. In the following paragraphs several existing reflection crack models will be discussed. Then, the focus will be placed on the SIF calculation and fracture properties of asphalt mixtures.

A. Reflection cracking models

1) Reflection cracking model proposed by Jayawickrama and Lytton (*12*)

As discussed previously, the combination of all three mechanisms of reflection cracking must be taken into account in order to accurately predict the development of reflection cracking. Based on research experience on modeling reflection cracking in the past two decades, TTI has found that the thermal stress is the main contributor to the occurrence of reflection cracking, followed by the shear mode, then by the bending mode. Based on this finding, Jayawickrama and Lytton (*12*) first proposed a combined reflection cracking model shown in Equation R-28. In this model, crack propagation calculated from Equation R-27 is repeated until the crack either stops growing for bending stress, or reaches the surface of the overlay for thermal tensile stress and/or shear stress. In this way the number of days for a crack to propagate in the bending, shearing or thermal mode is calculated separately. Then, the three modes of reflection cracking

are combined together to predict the actual number of days for a reflected crack to appear at the surface of the overlay.

$$N_f = N_{T1}\left(\alpha_1 - \alpha_2 * \frac{N_{T1}}{N_b} - \alpha_3 * \frac{N_{T1}}{N_{s1}}\right) + N_{T2}\left(\alpha_4 - \alpha_5 * \frac{N_{T2}}{N_{s2}}\right) \quad \text{(R-28)}$$

where:

N_f = Actual number of days for a reflection crack to reach the surface of the overlay,

N_{T1}, N_{T2} = Number of days for a thermal reflection cracking to reach the neutral axis (N_{T1}) and the additional number of days for thermal reflection cracking to break through the overlay (N_{T2}),

N_b = Number of days for bending reflection cracking to reach the neutral axis. The "neutral axis" is the point where bending stresses no longer cause crack propagation. Its location depends on the level of load transfer and moduli of pavement layers,

N_{s1}, N_{s2} = Number of days for shearing reflection cracking to reach the neutral axis (N_{s1}) and from there to break through the overlay (N_{s2}), and

α_1- α_5 = Calibration factors.

It is known that the crack propagation length is related to the total amount of cracking that reaches the overlay surface by way of a crack length distribution function. The idea is that material variability along the length of the pavement section will result in different crack propagation length, even for the same exposure conditions. The crack length distribution governs how much cracking is observed in a particular section that has a specific crack length computed on the basis of average material properties. Jayawickrama and Lytton (*12*) proposed an S-shaped empirical model (see Equation R-29) to describe the severity development of reflection cracking in an asphalt overlay. This reflection cracking severity model is based on the number of load repetitions (or days). Combining with the Equation R-28, Jayawickrama and

Lytton (*12)* developed three sets of calibration factors (α_1- α_5) for three levels of severity of reflection cracking: 0.33, 0.40, and 0.50, corresponding to low, medium, and high severity levels. Figure R-17 shows an example of the prediction results from Jayawickrama and Lytton's model. It should be also note that it is the only model that dealt with reflection cracking severity.

$$g = e^{-\left(\frac{\rho}{N}\right)^{\beta}} \qquad \text{(R-29)}$$

where:

g = Damage rating of the pavement, ranging from 0 to 1.
N = Number of load repetitions (or days).
ρ, β = Calibration coefficients.

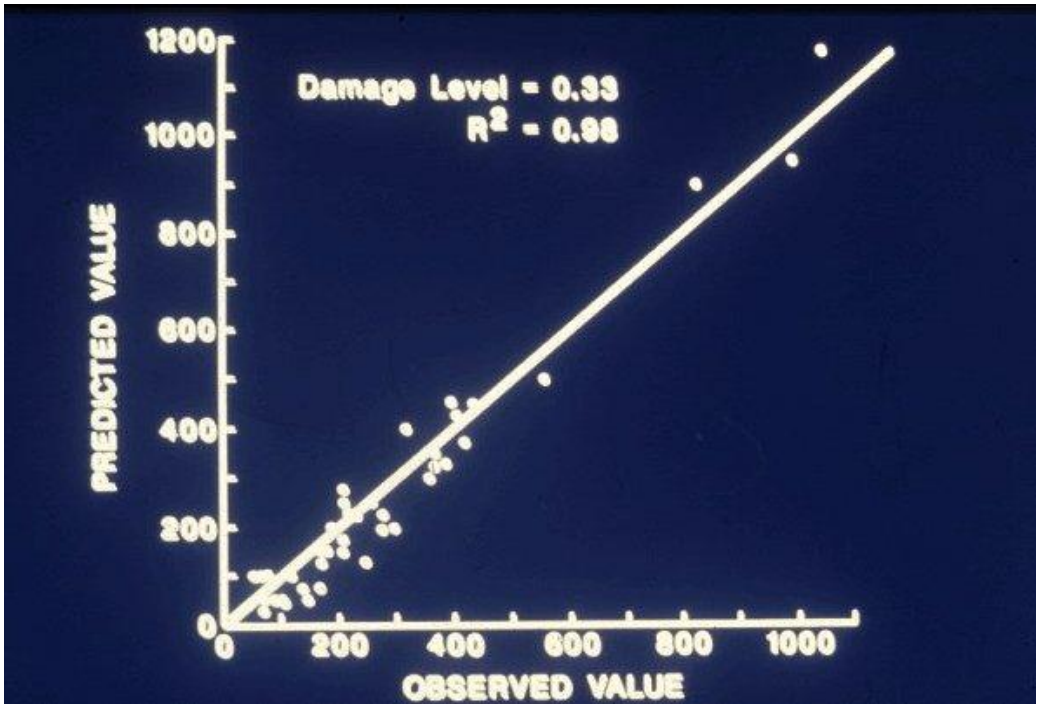

Figure R-17. Predicted vs. observed reflection cracking (Days) (12).

2) Reflection cracking model proposed by Owusu-Antwi, et al. (*49*)

Owusu-Antwi et al. (*49*) also developed a mechanistic based reflection cracking model for asphalt concrete-overlaid pavements. They also used the Paris' law (Equation R-26) to describe crack propagation. Then, a similar form of Equation R-27 was used to estimate the number of load repetitions (N_i) needed to propagate a crack through an asphalt overlay of thickness, h_{OL}. However, a simplified approximation, as expressed in Equation R-30, was proposed to estimate N_i. For any level of temperature or traffic loads with known K_C, the number of load applications to failure N_i can be calculated. With N_i known, the contribution of each load application to the total damage can then be determined.

$$N_i = \frac{h_{OL}}{AK_C{}^n} \qquad \text{(R-30)}$$

where:

N_i = Number of load repetitions (N_i) needed to propagate a crack through the asphalt overlay thickness, $h_{OL,}$

h_{OL} = Asphalt overlay thickness,

K_C = Stress intensity factor at the crack tip when the crack has propagated to the middle of the asphalt concrete overlay, and

A, n = Material constants determined experimentally.

- ***Reflection cracking damage model***

With known K_C induced by temperature variation, A, and n, the number of temperature load applications to failure N_{temp} can be calculated from Equation R-30 for any composite asphalt concrete-overlaid pavement. The damage accumulated from temperature variation is then calculated as follows:

$$TEMPDAMAGE = \frac{AGE}{N_{temp}} \qquad \text{(R-31)}$$

where:

AGE = Age of the pavement after overlay, in years, and
N_{temp} = Number of temperature load applications to failure.

For each axle load level *i*, the number of applications to failure $N_{i,\ traffic}$ can also be estimated from Equation R-30. The damage accumulated from traffic load can then be calculated as follows using Miner's cumulative damage approach. It should be noted that only mode II shearing loading was considered in the Owusu-Antwi et al. model (*49*).

$$TRAFDAMAGE = \sum \frac{n_i}{N_i} \quad \text{(R-32)}$$

where:

n_i = Actual number of axle passes for axle weight *i*, and
N_i = Allowable number of axle passes calculated from Equation R-30.

Then, the total damage, DAMTOT, from both temperature and traffic loading was calculated using the Equation R-33 obtained after calibration of the model with the long term pavement performance (LTPP) GPS-7 data, where n_i, AGE, N_i, and N_{temp} are defined before, and FI is the freezing index.

$$DAMTOT = 0.0132 \sum \frac{n_i}{N_i} + \frac{AGE}{N_{temp}} \left(8.79 + 0.000795 * FI * AGE\right) \quad \text{(R-33)}$$

- ***Reflection cracking amount model***

With the above total damage model (Equation R-33), Owusu-Antwi, et al. (*49*) developed the following Equation R-34 through optimization techniques to predict the percentage of reflection cracking, %RCRACKS, in a composite asphalt concrete-overlaid pavement. The

R-squared for this model is 61 percent. The predicted vs. measured reflection cracking on the 33 LTPP GPS-7 sections is plotted in Figure R-18.

$$\%RCRACKS = \frac{100 * DAMTOT^{1.9}}{DAMTOT^{1.9} + 1} \quad \text{(R-34)}$$

3) Simplified overlay design model proposed by Al-Qadi and his associates (*50, 88*)

Al-Qadi and his associates developed a simplified overlay design model to predict the service life of rehabilitated flexible pavement structures against reflective cracking, which was based on linear elastic fracture mechanics principles (*50, 88*). It was assumed that reflection cracking occurrence include three stages: crack initiation, crack stable propagation, and crack unstable propagation. The last stage was neglected because the crack growth rate increases rapidly in this stage as global instability is approached. Thus, both crack initiation and crack propagation stages were considered by A-Qadi and his associates (*50, 88*). The crack initiation phase is described using a traditional fatigue law (Equation R-35) developed by the Belgium Road Research Center (89), and the crack propagation phase is described using Paris's law (Equation 26). Three contour lines were used around the crack front to calculate the path independent J-integral. Then, calculations of the stress intensity factors were determined based on the J-integral using 3-D commercial FE software ABAQUS 5.8-1 (*50, 88*).

$$N = 4.856 \times 10^{-14} \gamma_{zx}^{-4.76} \quad \text{(R-35)}$$

where:

N = Number of cycles before crack initiation, and

γ_{zx} = Shear strains 10mm above the existing crack.

The total number of cycles before a crack reflects to the pavement surface is defined as follows (assuming that global instability is reached when the crack front is at 12.7 mm from the pavement surface):

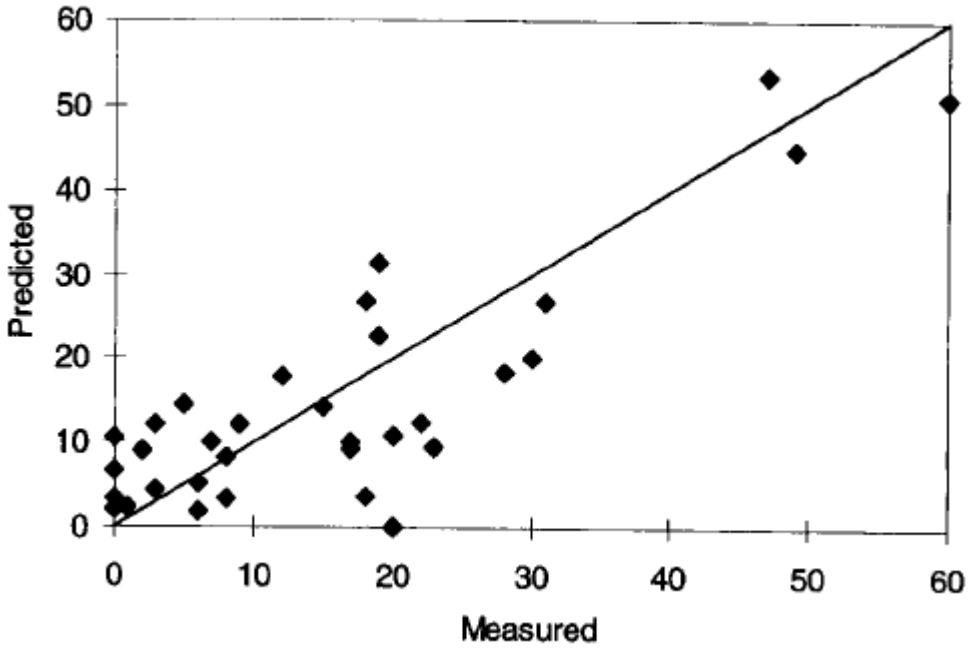

Figure R-18. Predicted vs. measured reflection cracking at LTPP GPS-7 sections (49).

$$N_{total} = N_{initiation} + N_{propagation} \quad \text{(R-36)}$$

where:

N_{total} = Total number of cycles before the crack reach 12.7 mm from the surface of the overlay,

$N_{initiation}$ = Number of cycles for crack initiation at the bottom of the overlay, and

$N_{propagation}$ = Number of cycles for the crack to propagate from the bottom of the overlay to 12.7mm from the surface of the overlay.

Although the above analysis is capable of effectively evaluating the overlay service life against reflective cracking, it is very time consuming. Thus, a simplified regression model was developed to predict the number of cycles as a function of the significant variables.

$$\log W_{t80} = \frac{1}{10^4}\left[255H_{overlay} + 2.08E_{overlay} + 45.3H_{HMA} + 8.73E_{HMA} + 1.34H_{base} + 6.93E_{base} + 1.49E_{subgrade}\right] \quad \text{(R-37)}$$

where:

W_{t80} = Total number of 80-kN single-axle load applications,
$H_{overlay}$ = Thickness of HMA overlay (mm),
$E_{overlay}$ = Modulus of resilience of HMA overlay (MPa),
H_{HMA} = Thickness of existing HMA layer (mm),
E_{HMA} = Modulus of resilience of existing HMA layer (MPa),
H_{base} = thickness of base layer (mm),
E_{base} = Modulus of resilience of base layer (MPa),
$E_{subgrade}$ = Modulus of resilience of subgrade (MPa), and

It should be kept in mind that the influence of temperature variations on reflection cracking was not taken into account in the above regression equation.

- ***Determination of SIF***

Since there is a singularity at the crack tip in the stress field, an FE program is needed to compute the SIF. Two special SIF computation programs have already been developed for crack propagation. The first one named CRACKTIP was developed for thermal cracking by Lytton and his associates (*52*) at the Texas Transportation Institute in 1976. The CRACKTIP is a 2-D FE program and it models a single vertical crack in the asphalt concrete layer via a crack tip element (*52*). This program has been successfully used to develop the SIF model and predict the cracking propagation. Figure R-19 shows the SIF of bending (SIF_b) and SIF of shearing (SIF_s) vs. crack length relationship. It is interesting to know that there is a "neutral axis" where bending stresses no longer cause crack propagation. Its location depends on the level of load transfer and the moduli of the pavement layers. This neutral axis must be considered in order to accurately predict reflection cracking. Actually, it was this program CRACKTIP that was successfully used in low-temperature cracking prediction under the SHRP A-005 research (*4*).

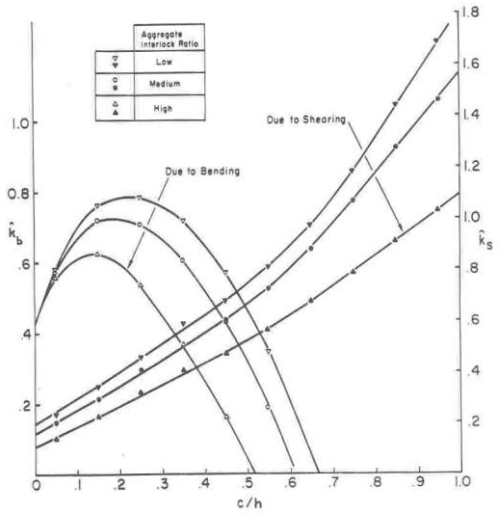

Figure R-19. Non-dimensionalized bending and shearing SIF vs. Non-dimensionalized crack length (12).

Another powerful SIF program named CAPA (Computer Aided Pavement Analysis) was developed by Delft University of Technology in 1990s (*53, 54, 90, 91*). The CAPA program was initially developed for reflection cracking analysis. It uses a quarter point triangular singular element (91) to produce the stress singularity at the crack tip as shown in Figure R-20. The SIFs (K_I and K_{II}) can then be elegantly determined based on the following equations (Equations R-38 and R-39) developed by Ingraffea and Manu (92), if the displacements of the crack tip nodes computed by the finite element analysis are correlated to those predicted by theory.

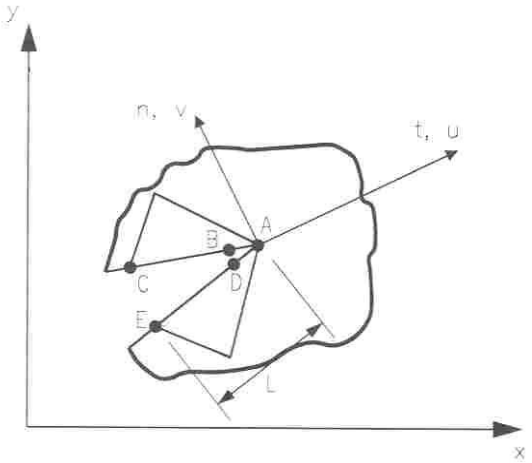

Figure R-20. Local axes crack-tip face modeling (54).

$$K_I = \sqrt{\frac{2\pi}{L}} \frac{G}{\kappa+1}\left[4(v_B - v_D) + v_E - v_C\right] \quad \text{(R-38)}$$

$$K_{II} = \sqrt{\frac{2\pi}{L}} \frac{G}{\kappa+1}\left[4(u_B - u_D) + u_E - u_C\right] \quad \text{(R-39)}$$

where:

G = Shear modulus,

κ = $(3-\upsilon)/(1+\upsilon)$ for plane stress,

κ = $3-4\upsilon$ for plane strain, and

L = element length.

The CAPA program has some special features that were created to specifically address the reflection cracking issue. All of these features make the CAPA program a good option for reflection cracking analysis and prediction.

1. Reflection cracking propagation was initially simulated in 2-D, and currently only in 3-D.
2. Special elements have been developed for the interlayer products. For example, a bar element (Figure R-21) was developed for the reinforcement grid.
3. An interface element (Figure R-21) was developed to simulate the crack interface or the interface between the overlay layer and the existing pavement (or between the reinforcement product and the surrounding asphalt concrete).
4. A powerful remeshing technique shown in Figure R-22 was incorporated into the CAPA program to completely, automatically simulate crack propagation.

The CAPA-3D program is a very powerful program to analyze the reflection cracking in asphalt overlays. Unfortunately, its high hardware and execution time demands render it suitable primarily for research purposes. 2-D and/or axisymmetric FE codes have lower demands in terms of hardware and execution times, however. Also, it is well known that the difference between plane strain conditions and the 3-D nature of a cracked geometry and loading leads to a

gross overestimation of the displacements for the same magnitude of external pressure loads. To solve this problem, a tailor made new finite element based system, named CAPAm, is specially developed which enables the efficient analysis of reflective cracking in asphalt overlays accounting for the 3-D nature of the cracked pavement geometry and the loading yet, it requires no more hardware and time resources that a 2-D FE analysis.

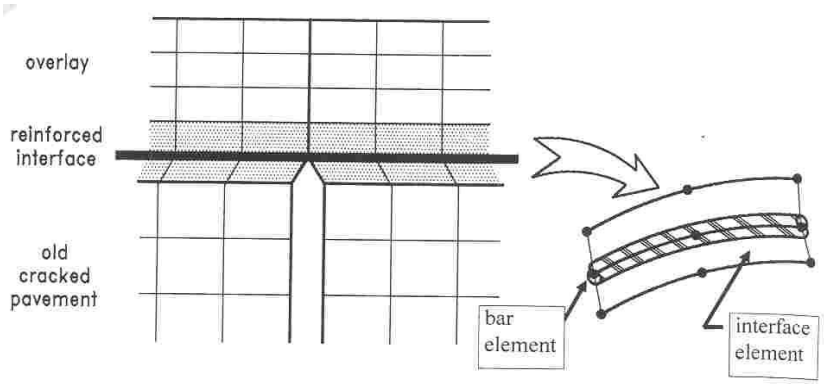

Figure R-21. Interlayer element (40).

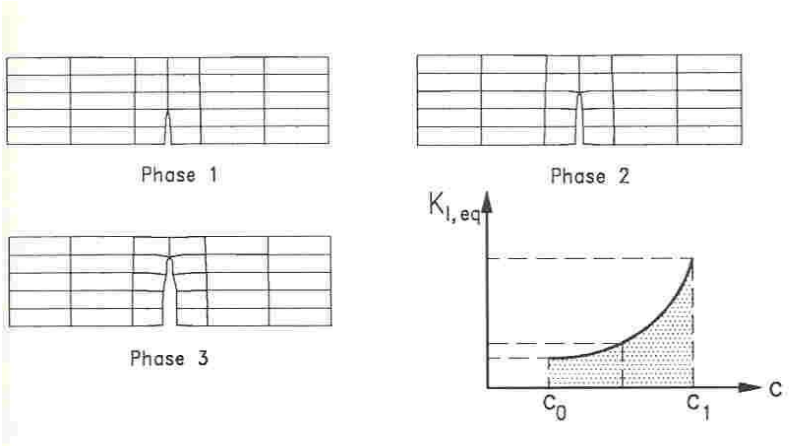

Figure R-22. Automatic crack propagation procedure in CAPA (91).

- ***Material Properties: A, n***

The use of Paris' law (Equation R-26) for the description of the crack growth process in visco-elastic materials, such as asphalt concrete mixes, has been theoretically justified by Schapery (*38, 39, 93*). Equation R-26 shows two material properties, A and n, which are the fracture properties of asphalt concrete mixes. First of all, Schapery (*38, 39, 93*) developed A and n equations in the 1970s based on viscoelastic theory. Laboratory tests characterizing fracture properties, A and n, of asphalt concrete mixes has also been conducted for a long time (*48, 83, 84, 85, 87, 94, 95, 96, 97, 98, 99, 100, 101, 102, 103*). Among them, the most systematic laboratory studies on A and n were conducted by Molenaar and his associates (*98, 99, 100, 101, 102, 103*). Thus, the proposed fracture properties of asphalt concrete mixes will be based on their work. Detailed information on their laboratory testing program can be found in references *99* and *101*. Only summary information is presented here. Tables R-4 and R-5 present the asphalt concrete mixes tested by Molenaar and Jacobs, which include sand asphalt (SA), open-graded asphaltic concrete, dense-graded mixes with/without modified binder, SMA, and base course mixes. Test and loading conditions are provided in Tables R-6, R-7, and R-8. Test results are tabulated in Tables R-9 and R-10.

Table R-4. Mix composition (99).

Mix	Gravel Sand Asphalt			Open Asphaltic Concrete				Sand Asphalt	Dense Asphaltic Concrete				Cold Asphalt
Composition (Percentage by weight)	A_1	A_2	A_3	B_1	B_2	B_3	B_4	C	E_1	E_2	E_3	E_4	F
Gravel	55	55	55	--	--	--	--	--	--	--	--	--	--
Crushed gravel	--	--	--	62	62	62	62	--	57	57	57	57	60
Riversand	39	19.5	9	31	--	31	--	63	--	--	9	9	--
Fore shore sand	--	19.5	30	--	31	--	31	31	35	35	--	--	--
Crushed riversand	--	--	--	--	--	--	--	--	--	--	26	26	31
Filler DP18 (weak)	6	6	6	7	7	7	7	--	--	--	--	--	--
Filler KHO (weak)	--	--	--	--	--	--	--	6	--	--	--	--	--
Filler Duras (medium)	--	--	--	--	--	--	--	--	8	8	8	8	--
Filler	--	--	--	--	--	--	--	--	--	--	--	--	3
Bitumen 45/60	5	5	5	--	--	5	5	4	6.4	--	6.4	--	--
Bitumen 80/100	--	--	--	5	5	--	--	--	--	6.4	--	6.4	--
Bitumen 80/100+ fluxoil	--	--	--	--	--	--	--	--	--	--	--	--	7.5
Mean Void Content (%)	5.04	7.57	10.01	4.95	9.98	3.72	9.09	20.5	7.08	6.84	2.9	4.39	3
Degree of Compaction (%)	97.2	97.1	96.5	97.7	96.5	99.0	97.5	97.0	95.4	96.4	98.7	97.2	
Location in Structure	Base			Binder Temporary Top layer				Subbase	Top layer				Top layer

Table R-5. Actual composition of the involved mixes (in percentage by volume; bitumen content in percentage by weight) (101).

Mix	SA	DAC8	DAC16										DAC mod	SMA
			A	B	C	D	E	F	G	H	I	J		
Crushed gravel														
2/6		21.4	11.0	10.6	10.9	11.1	11.0	10.8	10.9	11.0		9.0	11.0	
2/8											22.4			
4/8		21.2	15.6	15.0	15.5	15.7	15.8	15.4	15.5	15.5		17.9	15.3	18.8
8/11			9.3	8.9	9.3	9.4	9.4	9.2	9.3	9.2		7.5	9.4	41.8
8/16											26.7			
11/16			13.6	13.1	13.5	13.7	13.8	13.4	13.6	13.5		14.3	13.7	
Riversand		4.3	4.4	4.2	4.4	4.5	4.5	4.3	4.3	3.9	4.5	4.6	4.4	3.2
Ysselmeer sand		2.9	2.9	2.8	2.9	2.9	2.9	2.9	3.1	2.8	3.1	3.1	3.0	3.2
Crushed riversand	60.9	19.9	21.1	20.2	21.0	21.4	21.4	20.8	21.7	19.9	20.9	21.9	20.7	6.0
Filler DF18 (weak)	10.1													
Filler Wigras 40K (weak)		6.7	5.6	5.4	5.6	5.7	5.7	5.5	4.4	6.6	5.7	5.6	5.8	
Filler Wigro (weak)														7.2
Bitumen 45/60	20.7													
Bitumen 80/100		15.7	15.4	14.7	15.3	14.1	14.7	16.4	15.1	15.1	16.4	15.3		16.7
Sealoflex SBF 5-60													14.7	
Anti Dripping Agent														0.1
Mean Void Content (%) σ_{n-1} Void Content (%)	8.3 1.9	7.9 0.3	1.1 0.4	5.1 0.9	1.6 0.3	1.5 0.4	0.8 0.2	1.3 0.2	2.0 0.3	2.3 0.4	0.3 0.1	0.8 0.3	2.0 0.4	3.0 0.9
Compaction Degree (%)	96.8	93.7	101.7	98.1	100.3	101.6	102.0	100.8	100.9	101.5	102.6	101.8	100.8	100.2
Bitumen content (%m/m)	10.0	6.8	6.2	6.2	6.2	5.7	5.95	6.7	6.2	6.2	6.2	6.2	6.0	7.0

Table R-6. Test conditions used in crack growth experiments (99).

Mix	5°C/10 Hz	15°C/10 Hz	15°C/1 Hz	25°C/1 Hz
A_1	X	X	X	X
B_1		X	X	
B_3	X		X	
E_4		X	X	
F	X		X	

Table R-7. Test and loading conditions of the mixes: SA, DAC8, DACmod, and SMA (101).

		Test situation:														
		1a	1b	1c	2a	2b	2c	3a	3b	3c	4a	4b	4c	5a	5b	5c
Temperature [^{0}C]		15	25	5	15	15	15	15	15	15	15	15	15	15	15	15
Frequency [Hz]		8	8	8	2	4	16	8	8	8	8	8	8	8	8	8
Estimated life span [hr]		1	1	1	?	?	?	0.5	2	4	?	?	?	?	?	?
Deformation level [μm]	SA	61	100	54	61	61	61	66	71	76	61	61	61	61	61	61
	DAC8	73	96	39	73	73	73	37	50	60	73	73	73	73	73	73
	DAC16	55	120	32												
	DACmod	190	220	82	190	190	190	160	170	180	190	190	190	190	190	190
	SMA	78	160	48	78	78	78	68	73	83	78	78	78	78	78	78
Sinusoidal loading with rest periods [s]		0	0	0	0	0	0	0	0	0	⅛	¼	1			
Only the tension pulse of sinus with rest period [s]														⅛	¼	1

Table R-8. Test and loading conditions of the DAC16 mix (101).

	Test situation											
	1a	1b	1c	2a	2b	3a	3b	3c	4a	4b	5a	5b
Temperature [^{0}C]	15	25	5	15	15	15	15	15	15	15	15	15
Frequency [Hz]	8	8	8	8	8	8	8	8	8	8	8	8
Estimated life span [hr]	1	1	1	?	?	?	?	?	?	?	?	?
Deformation level [μm]	55	120	32	55	55	55	55	55	55	55	55	55
Compaction degree [%]	101.7	101.7	101.7	98.1	100.3	101.6	102.0	100.8	100.9	101.5	102.6	101.8
Percentage bitumen [%m/m]	6.2	6.2	6.2	6.2	6.2	5.7	5.95	6.7	6.2	6.2	6.2	6.2
Percentage air voids [%v/v]	1.1	1.1	1.1	5.1	1.6	1.5	0.8	1.3	2.0	2.3	0.3	0.8
Percentage filler [%m/m]	5.6	5.6	5.6	5.4	5.6	5.7	5.7	6.5	5.5	7.5	6.5	6.5
Kind of aggregate	mor	mor	mor	mor	mor	mor	mor	mor	mor	mor	porf	gran
Mix code	A	A	A	B	C	D	E	F	G	H	I	J

Table R-9. Test results (99).

Mix	temp [°C]	freq [Hz]	E [MPa]	c.v.	log k_1	n_1	log k_2	n_2	k_3	n_3	A	n	void content [%]	c.v.
A_1	25	1	1939	15.6	- 4.386	-2.02	1.686	-2.957	4.798	-1.281	6.394E- 5	2.889	5.76	13.7
	15	1	4089	27.0	- 7.670	-3.014	3.581	-4.246	6.549	-2.387	8.984E- 8	4.026	5.85	12.8
	15	10	8426	31.7	- 9.657	-3.571	4.245	-3.546			1.009E- 9	4.367	5.57	12.9
	5	10	8937	32.2	-12.917	-4.348	4.088	-4.63			5.035E- 9	3.086	6.38	5.6
B_1	15	1	2730	8.1	- 6.997	-2.756	2.392	-3.145	5.43	-1.539	1.673E- 6	3.787	4.72	22.5
	15	10	7951	34.6	- 9.701	-3.308	3.436	-2.611			9.183E- 7	2.882	5.17	11.8
B_3	15	1	4260	12.7	-13.206	-4.487	2.795	-4.876	6.459	-2.175	1.546E- 8	4.767	3.87	16
	5	10	17449	32.2	-17.908	-5.405	5.823	-6.803			2.612E-16	8.696	3.57	15.5
B_4	15	1	2612	11.9	- 6.692	-2.744	2.605	-3.194	5.775	-1.548	3.059E- 6	3.239	4.53	15.1
	15	10	4963	21.2	- 5.82	-2.342	2.799	-2.392			1.403E- 6	2.571	4.24	12.7
F	15	1	238	20.6	- 3.909	-1.842	-0.209	-2.328	3.591	-1.216	4.91 E- 3	2.994		
	5	10	2404	21.5	- 4.682	-1.938	1.778	-1.965			5.161E- 4	1.255		

Table R-10. The average A- and n-values per test situation (n. d.= not determinable) (101).

Test	SA		DAC8		DAC16		DACmod		SMA	
	n	A	n	A	n	A	n	A	n	A
1a	4.66	$3.27 \cdot 10^{-8}$	4.55	$6.89 \cdot 10^{-8}$	4.04	$8.06 \cdot 10^{-8}$	3.72	$1.52 \cdot 10^{-7}$	4.15	$1.97 \cdot 10^{-7}$
1b	4.32	$3.25 \cdot 10^{-6}$	3.88	$5.03 \cdot 10^{-7}$	3.53	$1.92 \cdot 10^{-5}$	2.8	$2.70 \cdot 10^{-6}$	3.15	$1.20 \cdot 10^{-6}$
1c	6.02	$6.08 \cdot 10^{-11}$	6.80	$4.38 \cdot 10^{-11}$	4.73	$1.52 \cdot 10^{-9}$	4.6	$3.30 \cdot 10^{-9}$	4.5	$7.46 \cdot 10^{-9}$
2a	4.43	$1.05 \cdot 10^{-7}$	4.00	$5.68 \cdot 10^{-7}$	3.63	$2.04 \cdot 10^{-7}$	3.6	$5.60 \cdot 10^{-7}$	3.6	$7.92 \cdot 10^{-7}$
2b	4.52	$4.93 \cdot 10^{-8}$	n.d.	n.d.	4.00	$1.02 \cdot 10^{-7}$	3.5	$6.23 \cdot 10^{-7}$	3.97	$2.85 \cdot 10^{-7}$
2c	4.77	$1.54 \cdot 10^{-8}$	n.d.	n.d.	n.d.	n.d.	4	$1.45 \cdot 10^{-7}$	4.65	$2.24 \cdot 10^{-8}$
3a	4.66	$3.27 \cdot 10^{-8}$	4.55	$6.89 \cdot 10^{-8}$	3.71	$1.78 \cdot 10^{-7}$	3.72	$1.52 \cdot 10^{-7}$	4.15	$1.97 \cdot 10^{-7}$
3b	4.66	$3.27 \cdot 10^{-8}$	4.55	$6.89 \cdot 10^{-8}$	3.89	$1.23 \cdot 10^{-7}$	3.72	$1.52 \cdot 10^{-7}$	4.15	$1.97 \cdot 10^{-7}$
3c	4.66	$3.27 \cdot 10^{-8}$	4.55	$6.89 \cdot 10^{-8}$	4.82	$2.34 \cdot 10^{-8}$	3.72	$1.52 \cdot 10^{-7}$	4.15	$1.97 \cdot 10^{-7}$
4a	n.d.	n.d.	4.55	$2.80 \cdot 10^{-8}$	3.50	$2.57 \cdot 10^{-7}$	3.72	$5.08 \cdot 10^{-8}$	4.15	$2.07 \cdot 10^{-8}$
4b	n.d.	n.d.	4.55	$2.03 \cdot 10^{-8}$	4.55	$3.39 \cdot 10^{-8}$	3.72	$1.47 \cdot 10^{-8}$	4.15	$2.22 \cdot 10^{-8}$
4c	n.d.	n.d.	4.55	$1.45 \cdot 10^{-8}$	n.d.	n.d.	n.d.	n.d.	n.d.	n.d.
5a	n.d.	n.d.	4.55	$3.71 \cdot 10^{-9}$	3.84	$1.48 \cdot 10^{-7}$	n.d.	n.d.	n.d.	n.d.
5b	n.d.	n.d.	4.55	$8.64 \cdot 10^{-9}$	3.08	$6.46 \cdot 10^{-7}$	n.d.	n.d.	n.d.	n.d.
5c	n.d.	n.d.	4.55	$3.33 \cdot 10^{-9}$	n.d.	n.d.	n.d.	n.d.	n.d.	n.d.

Schapery (*38, 39, 93*) presented a relationship between the crack growth velocity due to mode I loading (opening mode due to normal stresses) and properties of the material in which the crack is propagating according to:

$$A = \frac{\pi}{6{\sigma_m}^2 I_1^2}\left(\frac{\left(1-\upsilon^2\right)D_2}{2\Gamma}\right)^{\frac{1}{m}}\left(\int_0^{\Delta t} w(t)^n\, dt\right) \qquad \text{(R-40)}$$

with:

$$n = 2\left(1+\frac{1}{m}\right) \qquad \text{(R-41)}$$

for stress (or force)-controlled tests, and

$$n = \frac{1}{m} \qquad \text{(R-42)}$$

for strain (or displacement)-controlled tests,

where

- σ_m = Maximum stress a material can withstand before separation of the material occurs,
- ν = Poisson ratio of the material,
- D(t) = Time dependent creep compliance; $D(t)=D_0+D_2t^m$,
- m = Slope of double-log creep compliance vs. time plot,
- Γ = Fracture energy defined as the work done on a material to increase the fracture surface by a unit area,
- I_1 = Result of the integration of stress near the crack tip. Its value is between 1 and 2. A brittle mix will have a value near 1 and a ductile mix will have a value near 2,
- Δt = Period of the load to complete one cycle of loading, and
- w(t) = Wave shape of the stress intensity factor, its value ranges between 0 and 1.

The main advantage of Schapery's theory is that the constants A and n can be found from material properties as listed above. These parameters can then be obtained from fairly simple

tests which implies that performing very time consuming fatigue tests to determine them experimentally might not be necessary. Furthermore, empirical relationships of fracture properties A and n can be developed based on Schapery's theory using Molenaar and his associates' laboratory test results, which are discussed as follows.

- ***A and n empirical regression equations***

First of all, Equation R-40 can be expressed in the following log form:

$$\log A = \log\frac{\pi}{6} - 2\log\sigma_m - 2\log I_1 + \frac{1}{m}\log\left(1-\upsilon^2\right) - \frac{1}{m}\log\Gamma + \frac{1}{m}\log D_2 + \log\left(\int w(t)^n\,dt\right) \quad \text{(R-43)}$$

The above Equation R-43 can be simplified step by step as in the following forms:

$$\log A = a_1 + a_2\log\sigma_m + a_3\frac{1}{m}\log\Gamma + a_4\frac{1}{m}\log D_2 \quad \text{(R-44)}$$

$$\log A = a_1 + a_2\log\sigma_m + a_3 n\log D_2 \quad \text{(R-45)}$$

$$\log A = a_1 + a_2\log\sigma_m + a_3 n\log|E^*| \quad \text{(R-46)}$$

where a_1-a_4 are coefficients determined by regression analysis. The other parameters are the same as those defined in Equations R-40-R-42.

Since there is an empirical relationship between tensile strength and dynamic modulus, the above Equation R-46 can be further simplified as follows. Also, it is more practical to relate A only with n and | E*|, since | E*| is the only asphalt mix property needed for the MEPDG.

$$\log A = a_1 + a_2\log|E^*| + a_3 n\log|E^*| \quad \text{(R-47)}$$

As mentioned previously, the laboratory tests conducted by Molenaar and his associates will be used to calibrate the above equation. Figure R-23 shows the analysis results with an

R squared value of 0.9023. Equation 48 is the final equation to estimate the fracture property of an asphalt mix, the Paris' Law coefficient, A:

$$\log A = 4.830744 - 2.058768 \log|E^*| - 0.280849 n \log|E^*| \quad R^2 = 0.9023 \qquad \text{(R-48)}$$

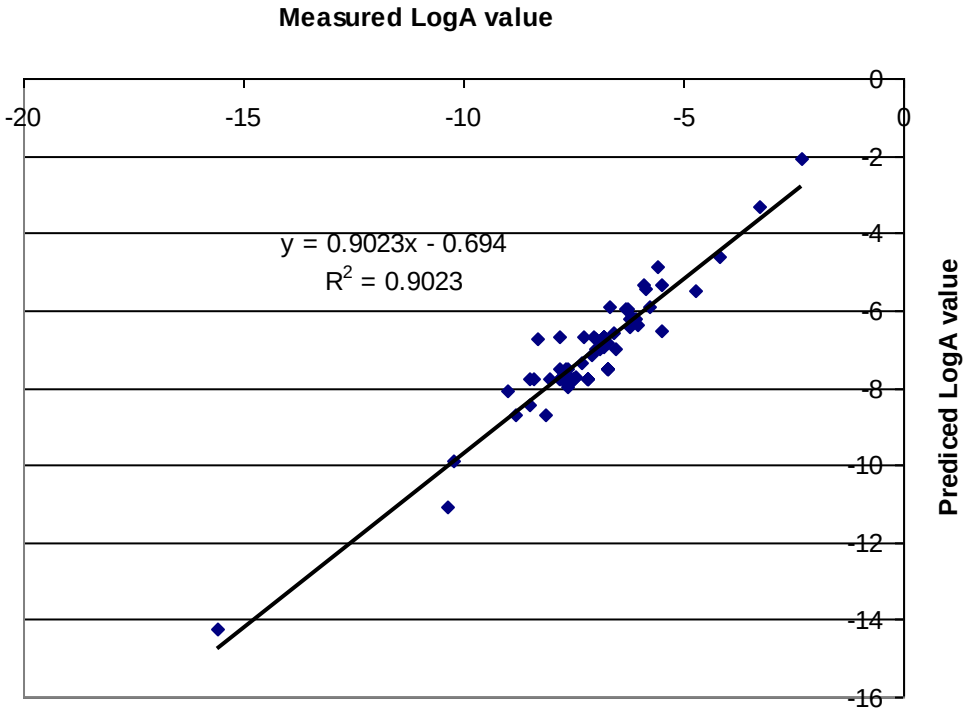

Figure R-23. Regression analysis of fracture property of asphalt mixes: A.

Regarding the fracture property of an asphalt mix *n*, Medani and Molenaar (*103*) compared the measured *n* with the estimated *n* values by Equation R-42. They found differences between these two values. This difference can be attributed to the limitations of the model as Schapery's theory is developed for an ideal visco-elastic material. This assumption is not fully applicable to asphalt mixes since they contain voids and aggregate particles which influence the crack growth. After analyzing the available data, a corrected model (Equation R-49) was recommended to estimate the *n* value.

$$n = \frac{2}{m\left(0.541 + \frac{0.346}{m} - 0.03524V_a\right)} \quad R^2=0.92 \qquad \text{(R-49)}$$

where m is the absolute value of the log-log slope of the stiffness with respect to loading time, and V_a is the air void content in percent.

In summary, the FE plus fracture mechanics based reflection cracking model is conceptually sound, and the three mechanisms of reflection cracking (bending, shearing, and thermal loading) can be easily described with a fracture mechanics based model. Furthermore, this type of model, as discussed previously, has been successfully employed to predict the reflection cracking in asphalt overlays by different researchers. Moreover, specific software such as CRACKTIP, CAPA-3D, CAPAm, are available for automatically calculating the SIF, which once was the most difficult part in the use of fracture mechanics. Another advantage of this type of model is that empirical equations, based on Schapery's theory, have been developed to estimate the fracture properties of asphalt concrete mixes. Thus, the FE plus a fracture mechanics based reflection cracking model, compared to the other models, is most suitable, as an adjunct to the MEPDG approach, to model reflection cracking in asphalt overlays.

6. Crack Band Model

Another way to model the behavior of an asphalt overlay on a cracked pavement structure that was used by Joseph et al. (104) is a blunt crack band theory based model (currently called crack band model [*105*]). The crack band model was developed based on the "smeared crack concept" introduced by Rashid (*106*). In this approach, a single discrete crack is replaced by infinitely many parallel cracks of infinitely small opening continuously distributed (smeared) over the finite element. Also, the effect of this smeared cracking can be modeled by reducing the material modulus in the direction normal to the cracks after the peak strength of the material has been reached.

Joseph et al. (*104*) discussed the reasonableness and necessity of the application of a crack band model to analyze low-temperature reflection cracking. First of all, asphalt concrete is a heterogeneous material. The general approximation procedure is that a heterogeneous material is represented by an equivalent homogeneous continuum, if its size is sufficiently large compared to the size of aggregates, voids, etc. in the material. The stresses and strains in the equivalent

homogeneous continuum are defined as the average of the micro stresses and micro strains over the selected representative volume which is shown in Figure R-24. This definition is based on the theory of randomly inhomogeneous materials (*107, 108*). It implies that the detailed distributions of stress or strain over distances less than the size of several aggregates are meaningless. Consequently, the geometry of the microstructure with the difference in the elastic constants between the aggregate and the binder is not taken into account. Only the stress resultants and the accumulated strain over the cross-section of the characteristic volume as represented by the crack band will be of interest.

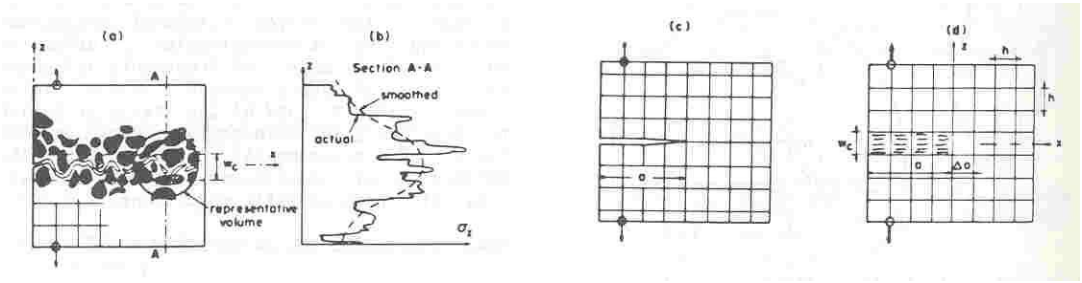

Figure R-24. Random microstructure, scatter of microstresses, and crack band or sharp crack model (106, 107).

Secondly, a straight line crack representation is an approximation. The actual crack path in concrete is not smooth but highly tortuous (see Figure R-24). The crack tends to curve around the hard aggregate pieces and randomly deviate to each side of the overall fracture axis by distances approximately equal to the aggregate size. The scatter in the location of visible microcracks relative to the path of crack propagation is better characterized by the crack band concept than the usual sharp crack approximation.

Thirdly, it has been proven (*107, 108*) that the line crack and the crack band models yield the same results for cases when the stress at failure drops suddenly to zero without undergoing any strain softening as a result of micro cracking. However, the assumption of abrupt stress drop is inadequate for cross-section dimensions that are not sufficiently large compared to the aggregate size (*107, 108*). Therefore, a gradual strain softening due to progressive micro

cracking must be taken into account and this can be done easily by using the concept of a crack band model.

Finally, the finite element method can be easily implemented particularly for crack propagation analysis. This can be done by simply reducing the material stiffness in the direction normal to the cracks in the band. In addition, this concept reflects the reality of densely distributed cracks in heterogeneous materials.

Based on the discussion above, Joseph et al. defined the effective width of an existing crack as shown in Figure R-25. Then, a 2-D plain strain FE model (see Figure R-26) was developed to analyze the effect of various treatments on retarding low-temperature reflection cracking. Figure R-27 presents the analysis results. It must be mentioned here that Joseph et al. used the crack band model only to analyze the induced thermal stress at the bottom of asphalt overlays. No crack propagation was ever tried in asphalt overlays by using the crack band model.

More intensive research is needed in order to implement this approach into predicting reflection cracking in asphalt overlays. Actually, the crack band model, as discussed in detail by Bazant and Planas (*105*), is equivalent to the cohesive cracking model. More discussion of this will be provided in the next section.

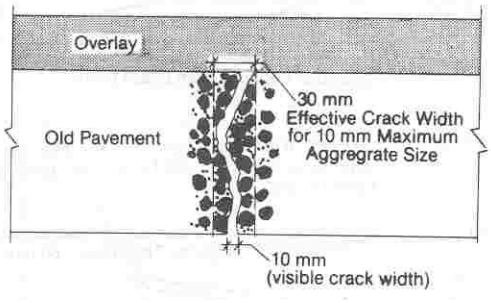

Figure R-25. Effective width of existing crack (105).

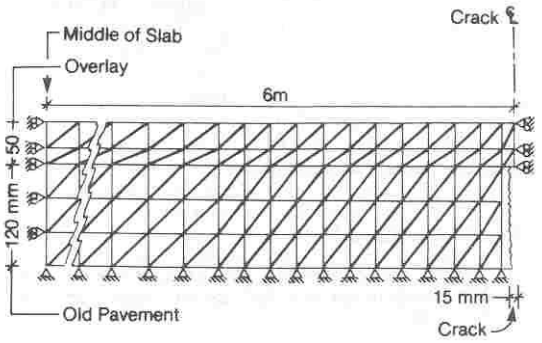

Figure R-26. Finite element model (104).

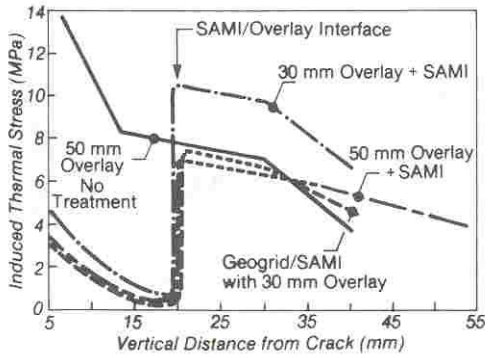

Figure R-27. Comparative effect of various treatments (104).

7. Cohesive Crack/Zone Model

It is well known that asphalt concrete is a not linear elastic material, and its cracking behavior is also complicated. Uzan and Levenberg (*109*) discussed the phenomenology of asphalt concrete fracture and provided a brief overview of the cohesive crack model (CCM). There is a strongly nonlinear fracture process zone (FPZ) around the crack tip in asphalt concrete as shown in Figure R-28. It is important to mention that in some situations, for asphalt concrete mixtures, the FPZ can extend to considerable lengths, up to a few centimeters (*110*). In order to account for a relatively large plastic yield zone ahead of a crack tip, Dugdale (*111*) and Barenblatt (*112*) proposed a "correction" for the classical linear elastic fracture mechanics. Their model approximated an elastic-plastic material behavior by applying closure stresses at the model-crack's tip. Hillerborg et al. (*113*) proposed a similar model to account for the relatively

large FPZ that has been encountered in concrete failure. The above models are generally considered Cohesive Cracking Models, because the models employ cohesive closure stresses at the near crack tip region.

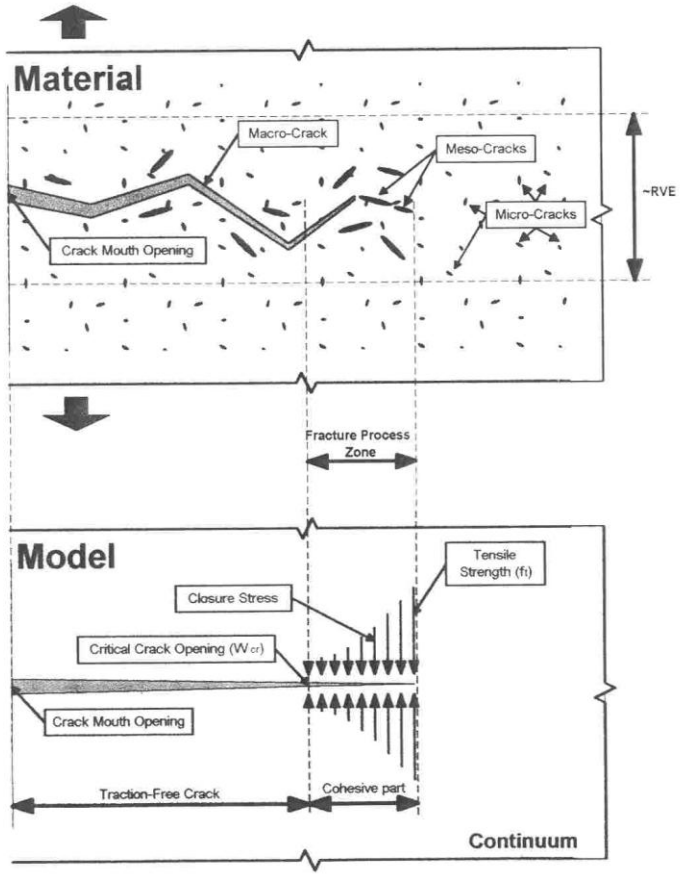

Figure R-28. Cohesive cracking model analogy (109).

The three fundamental hypotheses of the standard cohesive crack model are as follows:

- The properties of the materials outside the process zone are governed by the undamaged state.
- A crack length can be divided into two separate regions (see Figure R-28): a traction free length, and a cohesive part. In the cohesive part, crack opening resisting tractions exist and there is still stress transfer between its faces, which is done by

introducing closure stresses. The CCM postulates that the cohesive part of the crack begins to form at a "point" when the maximum principal stress at that "point" reaches the tensile strength of the material (and the crack propagation is perpendicular to the maximum stress direction) (*109*). Actually, this postulation is a crack initiation criterion.

- Meanwhile, the stress transfer capability of the cohesive part follows a descending path, from full transfer capability (when the cohesive crack faces just begin to depart (say peak stress conditions)) down to zero transfer capability as the displacement between the two cohesive crack faces reach a critical opening. This representation constitutes the CCM's crack propagation criterion. During the crack propagation analysis, the traction free crack is incrementally advanced whenever the calculated displacement reaches the critical opening in size. The stress transferred between the faces of the crack is described by a post-peak function (softening function). In the case of the opening mode, the function is:

$$\sigma = f(w) \qquad \text{(R-50)}$$

where σ is the tensile stress and *w* is the crack opening displacement. This softening curve of the material is considered to be a main component of the cohesive crack model. Although each material has its unique softening curve, determined only by experiments, Petersson (*114*) first found that the softening curve is similar in shape for different mixtures of Portland cement concrete when the softening curves are plotted in a non-dimensional form.

Jenq and his associates (*110, 115*) first applied the CCM to simulate crack initiation and propagation in asphalt concrete mixtures. However, their work got little attention until the Superpave model team started to develop an advanced asphalt concrete mixture material characterization model (*116*). Then, Uzan and Levenberg (*109*) developed a laboratory experimental test (direct tension test) to determine the CCM parameters. Similar work was later done by Seo et al. (*117*). Soares, et al. (*118*) considered the heterogeneity in crack modeling of asphalt concrete mixtures. The latest research in this field is being led by Paulino, Buttlar and

their associates (*119, 120, 121, 122*). Their research focus is on developing a laboratory test such as a disk-shaped compact tension test to determine the CCM parameters and associated numerical simulation. Repeated load testing has not been touched yet.

In general, the application of the CCM to asphalt concrete mixtures is still in the preliminary stage. All studies discussed above only applied the CCM to cracking under monotonic loading. To extend the CCM to repeated loading (such as reflection cracking), additional material parameters describing damage accumulation under unloading and reloading are needed. However, no work on this has been done yet. Therefore, the CCM is very promising, but it is not mature yet. More development is still needed.

8. Non-local Continuum Damage Mechanics Based Reflection Cracking Model (123)

The most recent research on modeling reflection cracking was conducted by Wu et al. (*123*). Continuum damage mechanics (CDM) allows one to describe the heterogeneous microprocesses involved during the straining of materials and structures at the macroscale. The basic theory of CDM can be found in papers by Chaboche [*124, 125).* However, the application of CDM to asphalt concrete mixes was pioneered by Lee and Kim [*126, 127*], followed by many other researchers, and it is still under development. The ultimate state of local CDM corresponds generally to macroscopic crack initiation upon which it becomes a crack propagation problem and should be considered in the framework of Fracture Mechanics. If local CDM is used to describe crack propagation, the spurious mesh dependency then comes into play. Fortunately, this mesh-dependency can be avoided by introducing non-local mechanics. A non-local continuum is a continuum in which the stress at a point depends not only on the strain history of the same point, but also on the strain history of the point's neighbor. Bazant and Jirasek (*128*) gave a comprehensive, state-of-the-research review of non-local formulations and provided a series of causes as well as motivations for introducing non-local continuum.

Non-local CDM is essentially an "enhancement" of local-CDM. Thus, the local-CDM is the first to be introduced below.

A. Local CDM

The stress-strain relationship for a linear elastic material with isotropic damage can be written as:

$$\sigma = (1-\omega)\mathrm{C} : \varepsilon \qquad \text{(R-51)}$$

where $C_{ijkl} = \lambda\delta_{ij}\delta_{kl} + \mu\left(\delta_{ik}\delta_{jl} + \delta_{il}\delta_{jl}\right)$ with $\lambda = \dfrac{E\nu}{(1+\nu)(1-2\nu)}$ and $\mu = \dfrac{E\nu}{2(1+\nu)}$ is the elasticity tensor and the scalar $\omega \in [0,1]$ represents the damage. Damage is defined such that ω= 0 represents the initial, undamaged material and ω= 1 represents a state of complete loss of integrity.

Equation R-36 is complemented by the damage evolution law:

$$\dot{\omega} = g(\omega,\tilde{\varepsilon})\left\langle \dot{\tilde{\varepsilon}} \right\rangle_{+} \qquad \text{(R-52)}$$

where ω is the time derivative of damage ω, $g(\omega,\tilde{\varepsilon})$ is a non-negative function to enforce the irreversibility of damage evolution, $\tilde{\varepsilon} = f(\varepsilon)$ is a measure of the strain that reflects its damaging effect due to cracking, and $\langle . \rangle_{+}$ denotes the Macaulay bracket which is an average over a representative volume.. A popular definition of $\tilde{\varepsilon}$ is given by Mazars and Cabot (*129*):

$$\tilde{\varepsilon} = \sqrt{\sum_{i=1}^{3} \langle \varepsilon_i \rangle_{+}^{2}} \qquad \text{(R-53)}$$

where ε_i is the i^{th} principal strain. When dealing with loading histories composed of well-defined, discrete cycles, an evolution law in terms of the number of cycles and the loading amplitudes is often considered more practical (*130*). Such a cycle-based damage evolution law can be obtained from Equation R-37 by integrating over one loading cycle resulting in a relation of the form (*131*):

$$\frac{\partial \omega}{\partial N} = G(\omega, \tilde{\varepsilon}_a) \qquad \text{(R-54)}$$

where N is the number of load cycles, $\tilde{\varepsilon}_a$ is the amplitude of $\tilde{\varepsilon}$ for the current load cycle, and G is a non-negative function representing the damage accumulation property of the material.

B. <u>Non-local CDM</u>

Numerous ways have been proposed to incorporate non-locality into the constitutive relations of materials. The most successful ones fall into two categories: integral formulation and implicit gradient formulation. The implicit gradient formulation was recommended since it is much easier to implement in the FE code, and it is a special case of the integral formulation.

Implicit gradient formulation is proposed by (*132*), in which a non-local strain $\bar{\varepsilon}$ is introduced to replace the local strain measure $\tilde{\varepsilon}$ in damage evolution Equations R-52 and R-54. And $\bar{\varepsilon}$ and $\tilde{\varepsilon}$ are related through an additional differential equation:

$$\bar{\varepsilon} - c\nabla^2 \bar{\varepsilon} = \tilde{\varepsilon} \qquad \text{(R-55)}$$

where $\sqrt{c}$ has a dimension of length and is related to the internal length scale which should be approximately equal to the maximum grain size of the material, and $\nabla^2 = \sum_i \partial^2 / \partial x_i^2$ is the Laplacian operator. Physically, Equation R-40 implies that $\bar{\varepsilon}$ is a spatial average of $\tilde{\varepsilon}$ and the radius of the averaging domain is in proportion to $\sqrt{c}$.

The introduction of Equation R-55 leads to a coupled problem between the displacement field and the non-local strain field. The non-local strain becomes an additional degree of freedom for each node. The evaluation of a consistent algorithmic tangent at any Gauss point requires only the current strain ε, damage ω, and non-local strain $\bar{\varepsilon}$ for that same point. In this sense, the implicit gradient formulation is mathematically local and is much easier to be incorporated into existing FE codes.

After developing the non-local CDM based reflection cracking model, the SHRP beam-fatigue tests were conducted to calibrate the model's parameters. Frequency sweep tests were used to determine the Young's modulus master curves of two asphalt concrete mixes.

Fatigue tests provided stiffness reduction curves that captured the material degradation process of the two asphalt concrete mixes under repetitive loading. FE models were established to simulate the beam fatigue test. Damage evolution law parameters were calibrated by matching the calculated and measured stiffness reduction curves. Finally, the laboratory calibrated reflection cracking model was verified by simulating reflection cracking in an HVS test conducted on an asphalt concrete overlay placed on a cracked and jointed concrete pavement. The model not only recovered the most dominant crack pattern observed in the field, but it also predicted the reflection cracking life of the overlay with reasonable accuracy. Figure R-29 shows the damage field and crack pattern after 396,000 load repetitions. In conclusion, the implicit gradient non-local CDM, implemented in a FE program, provides a promising mechanistic model for simulating reflection cracking in asphalt concrete overlays.

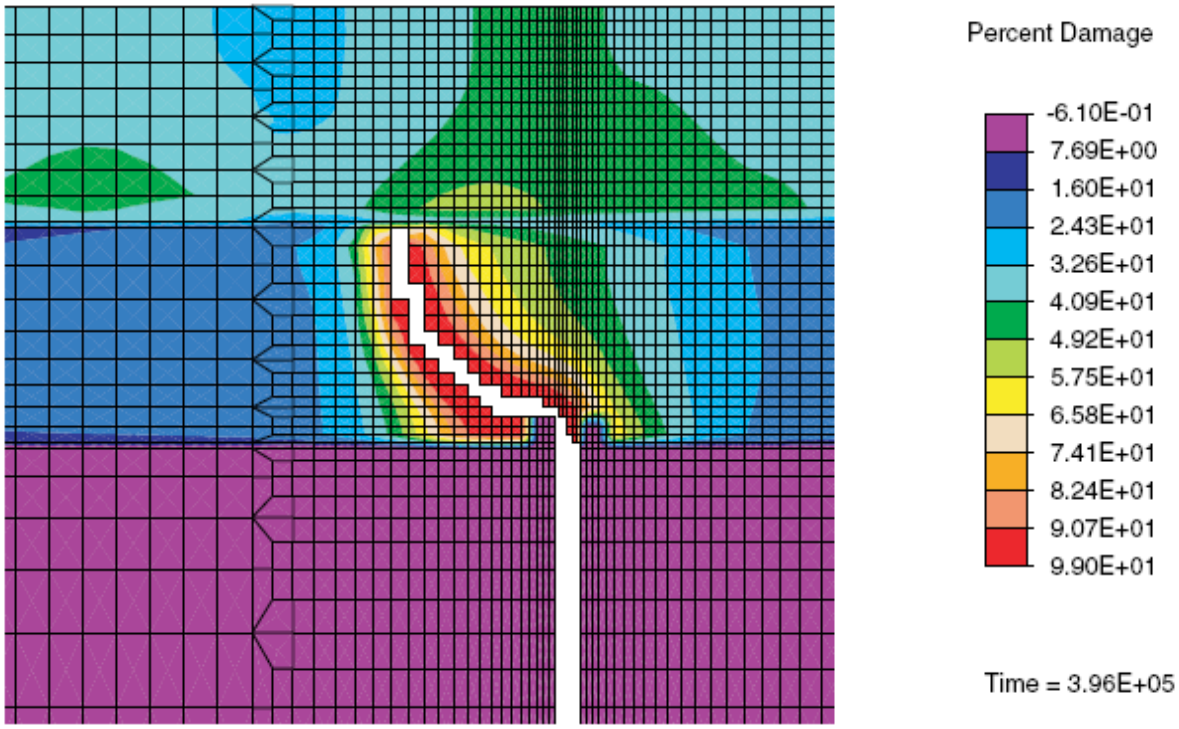

Figure R-29. Case 9, damage field and crack pattern after 396,000 load applications (132).

In addition, Wu (*82*) also proposed a mechanistic-empirical design procedure against reflection cracking in asphalt concrete overlays. This procedure is intended to be used in routine design and the user is not required to know the inner workings in the FE program. The flow chart of this procedure is displayed in Figure R-30. As shown in Figure R-30, the proposed asphalt overlay design procedure depends on the following three models: 1) the statistical critical strain model, 2) the regression model that links the initial conditions of an asphalt overlay to its crack through time N_{CDM}, and 3) the model for calculating the shift factor C accounting for traffic wander, aging, etc. The first model involves extensive linear elastic FE analyses. The second model requires the use of the first model as well as collecting damage evolution law parameters for typical asphalt concrete mixes and running FE simulation with non-local CDM constitutive model for thousands of overlay structures. The third model requires the use of the first two models as well as collecting extensive field performance data. Wu (*82*) just established the first statistical critical strain model. The other two models were left for future study.

In general, the non-local CDM reflection cracking model, similar to the CCM discussed previously, is very advanced. Wu's research results (*82*) demonstrated this promising model to predict reflection cracking in asphalt overlays over existing pavements. However, this non-local CDM model is still under development, and not ready for routine use. Also, the proposed asphalt overlay thickness procedure only considered reflection cracking caused by traffic loading.

REFLECTION CRACKING MODELS COMPARISON

Table R-11 presents a simple comparison among the eight types of reflection cracking models based on several parameters, such as the capability of handling the influence factors of reflection cracking and compatibility to the MEPDG. Obviously, the empirical approach is the simplest but the most inaccurate approach. The extended multi-layer linear elastic system and the equilibrium equation approaches are not compatible with the MEPDG. The crack band model, cohesive crack/zone model, and non-local continuum damage mechanics model are very advanced models, and the current status of these advanced models is that they are still under development, and not ready for being used yet. Thus, the two types of models that remain are FE plus beam fatigue law and FE plus fracture mechanics. FE plus beam fatigue law model cannot directly consider the three mechanisms of reflection cracking. Also, as discussed

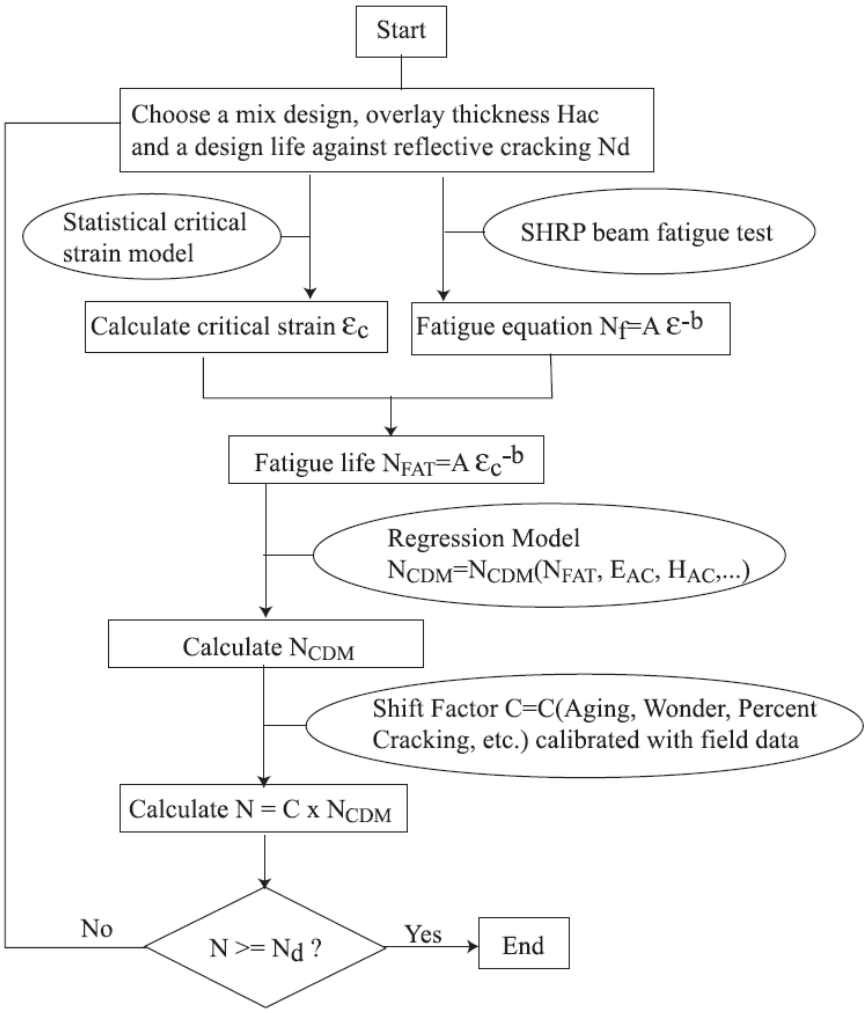

Figure R-30. Flow chart of the proposed overlay design procedure against reflective cracking (82).

previously, Wu (*82*) compared the N_{FAT} (the fatigue life of asphalt overlay calculated by the fatigue equation) and N_{CDM} (the crack through time of the overlay calculated by FE simulation with an advanced non-local continuum damage mechanics model). A weak relationship was found between N_{FAT} and N_{CDM}. This result indicates the necessity and importance of considering the crack propagation. Compared to the empirical and FE plus beam fatigue law approaches, the FE plus fracture mechanics approach is not too complicated. Furthermore, the FE plus fracture mechanics approach has been successfully employed to accurately predict reflection cracking of asphalt overlays by different researchers, and is fully compatible with the MEPDG. Thus, the FE

plus fracture mechanics approach is expected to produce the most useful results in the NCHRP 1-41 project, and was the available model judged to be the most likely to successfully achieve the objectives of this project.

Table R-11. Comparison of reflection cracking modeling approaches.

Model	Development status	Crack Propagation Mechanisms			Combined Mechanisms	Crack Prediction Method			Predicted Distress				Compatible with MEPDG	
		Thermal	Bending	Shearing		Fracture Mechanics	Phenomenological (beam) fatigue law	Empirical	Area		Severity		Yes	No
									Time	Traffic	Time	Traffic		
Empirical equation	Finished							√	√					√
Extended Multilayer linear elastic	Finished		√							√				√
Equilibrium equations	Finished	√	√	√				√		√				√
FE + fracture mechanistic	Finished	√	√	√	√	√			√	√		√	√	
FE + beam fatigue law	Finished		√				√		√				√	
Crack band theory	Under developing	√				√								√
Cohesive cracking model	Under developing		√			√								√
Non-local continuum damage mechanics model	Under developing		√	√		√								√